



Evidence for the spin-0 nature of the Higgs boson using ATLAS data [☆]



ATLAS Collaboration ^{*}

ARTICLE INFO

Article history:

Available online 16 August 2013

Editor: W.-D. Schlatter

Keywords:

Higgs boson

Spin

Parity

ABSTRACT

Studies of the spin and parity quantum numbers of the Higgs boson are presented, based on proton–proton collision data collected by the ATLAS experiment at the LHC. The Standard Model spin–parity $J^P = 0^+$ hypothesis is compared with alternative hypotheses using the Higgs boson decays $H \rightarrow \gamma\gamma$, $H \rightarrow ZZ^* \rightarrow 4\ell$ and $H \rightarrow WW^* \rightarrow \ell\nu\ell\nu$, as well as the combination of these channels. The analysed dataset corresponds to an integrated luminosity of 20.7 fb^{-1} collected at a centre-of-mass energy of $\sqrt{s} = 8 \text{ TeV}$. For the $H \rightarrow ZZ^* \rightarrow 4\ell$ decay mode the dataset corresponding to an integrated luminosity of 4.6 fb^{-1} collected at $\sqrt{s} = 7 \text{ TeV}$ is included. The data are compatible with the Standard Model $J^P = 0^+$ quantum numbers for the Higgs boson, whereas all alternative hypotheses studied in this Letter, namely some specific $J^P = 0^-, 1^+, 1^-, 2^+$ models, are excluded at confidence levels above 97.8%. This exclusion holds independently of the assumptions on the coupling strengths to the Standard Model particles and in the case of the $J^P = 2^+$ model, of the relative fractions of gluon-fusion and quark–antiquark production of the spin-2 particle. The data thus provide evidence for the spin-0 nature of the Higgs boson, with positive parity being strongly preferred.

© 2013 CERN. Published by Elsevier B.V. All rights reserved.

1. Introduction

In 2012 the ATLAS and CMS Collaborations published the discovery of a new resonance [1,2] in the search for the Standard Model (SM) Higgs boson H [3–8]. The present experimental challenge is to compare its properties with the SM predictions for the Higgs boson. In the SM, the Higgs boson is a spin-0 and CP-even particle ($J^P = 0^+$). The Landau–Yang theorem forbids the direct decay of an on-shell spin-1 particle into a pair of photons [9, 10]. The spin-1 hypothesis is therefore strongly disfavoured by the observation of the $H \rightarrow \gamma\gamma$ decay. The CMS Collaboration has published a spin–parity study [11] based on the $H \rightarrow ZZ^*$ channel where the SM scalar hypothesis is favoured over the pseudoscalar hypothesis at a confidence level (CL) above 95%.

In this Letter the $J^P = 0^+$ hypothesis of the SM is compared to several alternative hypotheses with $J^P = 0^-, 1^+, 1^-, 2^+$. The measurements are based on the kinematic properties of the three final states $H \rightarrow \gamma\gamma$, $H \rightarrow ZZ^* \rightarrow 4\ell$ and $H \rightarrow WW^* \rightarrow \ell\nu\ell\nu$, where ℓ denotes an electron or a muon. For the alternative hypotheses leading order (LO) calculations are used to predict the kinematic properties. To improve the sensitivity to different spin–parity hypotheses, several final states are combined. To test the 0^- spin–parity hypothesis, only the $H \rightarrow ZZ^*$ decay mode is used, while for the 1^+ and 1^- hypotheses the $H \rightarrow ZZ^*$ and $H \rightarrow WW^*$ channels are combined. For the 2^+ study, all three decay modes are

combined. It is assumed that only one single resonance contributes to the various decay modes considered in each combination.

The full dataset collected at $\sqrt{s} = 8 \text{ TeV}$, corresponding to an integrated luminosity of 20.7 fb^{-1} , is analysed for all three channels. For the $H \rightarrow ZZ^*$ decay mode, a dataset corresponding to an integrated luminosity of 4.6 fb^{-1} collected at $\sqrt{s} = 7 \text{ TeV}$ is also included.

While for the SM Higgs boson the Lagrangian structure and its couplings are fully determined, the alternative hypotheses can be described by a wide variety of models, characterised by different structures and effective couplings. Several approaches to describe such signatures can be found in the literature [12–17]. In this Letter, the alternative model descriptions are based on Ref. [12], as described in Section 2. In Ref. [12], the production and decay of a generic boson with various J^P quantum numbers are described by defining the most general amplitudes consistent with Lorentz invariance, angular-momentum conservation, Bose symmetry and the unbroken symmetry of the $SU(3) \times SU(2) \times U(1)$ gauge group.

This Letter is published together with another one [18] reporting the ATLAS measurements of the couplings of the Higgs boson derived from the observed signal production and decay rates. In that Letter the measurement of the mass of the Higgs boson, based on the invariant mass spectra in the $H \rightarrow \gamma\gamma$ and $H \rightarrow ZZ^* \rightarrow 4\ell$ final states, is also reported. On the basis of that measurement, the observed final states are assumed to be produced in the decay of a single particle with a mass of 125.5 GeV [18]. The definitions of the physics objects used in the analyses, the simulation of the different backgrounds and the main systematic uncertainties are described in Ref. [18]. This Letter reports only aspects specific to

[☆] © CERN for the benefit of the ATLAS Collaboration.

^{*} E-mail address: atlas.publications@cern.ch.

the spin and parity analyses. The ATLAS Collaboration has made public a collection of conference notes that document in detail the analyses reported in this Letter [19–21].

The outline of this Letter is as follows: Section 2 describes the spin–parity models considered in all three channels and the signal Monte Carlo (MC) simulation samples used in the analyses. The statistical procedure used to test the different spin–parity hypotheses is presented in Section 3. Sections 4, 5 and 6 provide brief descriptions of the spin–parity analyses in the $H \rightarrow \gamma\gamma$, $H \rightarrow ZZ^*$ and $H \rightarrow WW^*$ decay modes. Finally, in Section 7, the combined results in terms of compatibility with several spin–parity hypotheses are presented.

2. Signal modelling and Monte Carlo samples

The interactions of spin-0, 1 and 2 resonances with Standard Model particles are described in Ref. [12] by Eqs. 2, 4 and 5 for bosons and by Eqs. 8, 9 and 10 for fermions. The choices of the boson and fermion couplings for the specific spin and parity models used in this analysis are presented in Table 1 of Ref. [12].

The implications of these choices are briefly summarised in the following. The quark–antiquark ($q\bar{q}$) annihilation production process is not considered in the case of $J^P = 0^-$, since its contribution is negligible compared to gluon fusion (gg). For the $J^P = 1^+$ and 1^- cases, only the quark–antiquark annihilation production process is considered, since the Landau–Yang theorem also forbids the production of a spin-1 particle through the fusion of two on-shell gluons. Given the large number of possible spin-2 models, a specific one, denoted by 2_m^+ from Table 1 of Ref. [12], was chosen. This choice corresponds to a graviton-inspired tensor with minimal couplings to SM particles. In the 2_m^+ boson rest frame, its polarisation states projected onto the parton collision axis can take only the values of ± 2 for the gluon-fusion process and ± 1 for the quark–antiquark annihilation process. For the spin-2 model, only these two production mechanisms are considered. The production of the 2_m^+ boson is dominated by the gluon-fusion process with a contribution, at leading order in quantum chromodynamics (QCD), of about 4% from quark–antiquark annihilation [16,17]. This proportion could be significantly modified by higher-order QCD corrections. Since the experimental observables are sensitive to different polarisations, the studies were performed for several production admixtures by normalising the samples produced with the two different production processes in order to obtain samples of events corresponding to fractions, $f_{q\bar{q}}$, of $q\bar{q}$ annihilation ranging from 0% to 100% in steps of 25%. In the following, this model is referred to as $J^P = 2^+$.

The production and decay of the SM Higgs boson via the dominant gluon-fusion process is simulated using either the JHU Monte Carlo generator [12] for the $H \rightarrow ZZ^*$ process or the POWHEG [22] Monte Carlo generator for the $H \rightarrow \gamma\gamma$ and $H \rightarrow WW^*$ processes, each interfaced to PYTHIA8 [23] for parton showering and hadronisation. The production and decay of the $J^P = 0^-, 1^+, 1^-$ and 2^+ resonances are modelled using the JHU generator, interfaced to PYTHIA8 for parton showering and hadronisation.

The transverse momentum (p_T) distributions for the gluon-fusion signals produced with the JHU generator, which is leading-order in QCD, are weighted to reproduce the POWHEG+PYTHIA8 spectrum. The latter was tuned to reproduce the re-summed calculation of the HqT program [24]. It was checked that the distributions of all kinematic variables used for the spin–parity determination are compatible between the two MC generators after the re-weighting is applied. For the production process via $q\bar{q}$ annihilation, no re-weighting is applied.

The much smaller contributions from other production processes, namely vector-boson fusion and associated production, are

also considered. For the $H \rightarrow \gamma\gamma$ channel, they are included in the analysis and simulated as described in Ref. [18]. For the $H \rightarrow ZZ^*$ channel, they are ignored because they do not affect the kinematic distributions used in the spin analysis. For the $H \rightarrow WW^*$ analysis, where only the $e\mu$ final state with no additional jet activity is considered, as described in Section 6, they contribute at a negligible level and are therefore ignored. It should be noted that for the resonance under study, dominant contributions via vector-boson fusion and associated production can be excluded based on the measurements presented in Ref. [18].

For the background processes, the simulated samples are the same as those used in the coupling analyses. A detailed list of the MC generators and samples is given in Ref. [18].

All MC samples are passed through a full simulation of the ATLAS detector [25] based on GEANT4 [26]. The simulation incorporates a model of the event pile-up conditions in the data, including the effects of multiple proton–proton collisions in in-time and nearby bunch crossings.

3. Statistical method

The analyses described in this Letter rely on discriminant observables chosen to be sensitive to the spin and parity of the signal while preserving the discrimination against the various backgrounds, as described in Sections 4, 5 and 6 for the three final states. A likelihood function $\mathcal{L}(J^P, \mu, \theta)$ that depends on the spin–parity assumption of the signal is constructed as a product of conditional probabilities over binned distributions of the discriminant observables in each channel:

$$\begin{aligned} \mathcal{L}(J^P, \mu, \theta) &= \prod_j^{N_{\text{chann.}}} \prod_i^{N_{\text{bins}}} P(N_{i,j} \mid \mu_j \cdot S_{i,j}^{(J^P)}(\theta) + B_{i,j}(\theta)) \times \mathcal{A}_j(\theta), \end{aligned} \quad (1)$$

where μ_j represents the nuisance parameter associated with the signal rate in each channel j . The symbol θ represents all other nuisance parameters. The likelihood function is therefore a product of Poisson distributions P corresponding to the observation of $N_{i,j}$ events in each bin i of the discriminant observable(s),¹ given the expectations for the signal, $S_{i,j}^{(J^P)}(\theta)$, and for the background, $B_{i,j}(\theta)$. Some of the nuisance parameters are constrained by auxiliary measurements through the functions $\mathcal{A}_j(\theta)$.

While for the SM Higgs boson the couplings to the SM particles are predicted, they are not known *a priori* for the alternative hypotheses, defined as J_{alt}^P . In order to be insensitive to such assumptions, the numbers of signal events in each channel and for each tested hypothesis are treated as an independent nuisance parameters in the likelihood.

The test statistic q used to distinguish between the two signal spin–parity hypotheses is based on a ratio of likelihoods:

$$q = \log \frac{\mathcal{L}(J^P = 0^+, \hat{\mu}_{0^+}, \hat{\theta}_{0^+})}{\mathcal{L}(J_{\text{alt}}^P, \hat{\mu}_{J_{\text{alt}}^P}, \hat{\theta}_{J_{\text{alt}}^P})}, \quad (2)$$

where $\mathcal{L}(J^P, \hat{\mu}_{J^P}, \hat{\theta}_{J^P})$ is the maximum likelihood estimator, evaluated under either the 0^+ or the J_{alt}^P spin–parity hypothesis. The $\hat{\mu}_{J^P}, \hat{\theta}_{J^P}$ represent the values of the signal strength and nuisance

¹ As explained in the following sections, the sensitivity for spin–parity separation is improved by a simultaneous fit to two discriminants in the $H \rightarrow \gamma\gamma$ and $H \rightarrow WW^*$ decay modes, while in the $H \rightarrow ZZ^*$ channel only one discriminant is used.

parameters fitted to the data under each J^P hypothesis. The distributions of the test statistic for each of the two hypotheses are obtained using ensemble tests (Monte Carlo pseudo-experiments). The generation of the pseudo-experiments uses the numbers of signal and background events in each channel obtained from maximum likelihood fits to data. In the fits of each pseudo-experiment, these and all other nuisance parameters are profiled, i.e. fitted to the value that maximises the likelihood for each value of the parameter of interest. When generating the distributions of the test statistic for a given spin–parity hypothesis, the signal strength μ is fixed to the value obtained in the fit to the data under the same spin–parity assumption. The distributions of q are used to determine the corresponding p_0 -values $p_0(0^+)$ and $p_0(J_{\text{alt}}^P)$. For a tested hypothesis J_{alt}^P , the observed (expected) p_0 -values are obtained by integrating the corresponding test-statistic distributions above the observed value of q (above the median of the $J^P = 0^+q$ distribution). When the measured data are in agreement with the tested hypothesis, the observed value of q is expected to be close to the median, corresponding to a p_0 -value around 50%. Very small values of the integral of the J_{alt}^P distribution, corresponding to large values of q , are interpreted as the data being in disagreement with the tested hypothesis in favour of the SM hypothesis. An example of such distributions is shown in Section 7 for the 0^+ and 0^- hypotheses.

The exclusion of the alternative J_{alt}^P hypothesis in favour of the Standard Model 0^+ hypothesis is evaluated in terms of the corresponding $\text{CL}_s(J_{\text{alt}}^P)$, defined as:

$$\text{CL}_s(J_{\text{alt}}^P) = \frac{p_0(J_{\text{alt}}^P)}{1 - p_0(0^+)}. \quad (3)$$

4. $H \rightarrow \gamma\gamma$ analysis

The $H \rightarrow \gamma\gamma$ decay mode is sensitive to the spin of the Higgs boson through the measurement of the polar angular distribution of the photons in the resonance rest frame. For this channel, the SM spin hypothesis is compared only to the $J^P = 2^+$ hypothesis. Spin information can be extracted from the distribution of the absolute value of the cosine of the polar angle θ^* of the photons with respect to the z -axis of the Collins–Soper frame [27]:

$$|\cos\theta^*| = \frac{|\sinh(\Delta\eta^{\gamma\gamma})|}{\sqrt{1 + (p_T^{\gamma\gamma}/m_{\gamma\gamma})^2}} \frac{2p_T^{\gamma 1} p_T^{\gamma 2}}{m_{\gamma\gamma}^2}, \quad (4)$$

where $m_{\gamma\gamma}$ and $p_T^{\gamma\gamma}$ are the invariant mass and the transverse momentum of the photon pair, $\Delta\eta^{\gamma\gamma}$ is the separation in pseudo-rapidity of the two photons, and $p_T^{\gamma 1}, p_T^{\gamma 2}$ are the transverse momenta of the photons.

This channel has a large background, dominated by non-resonant diphoton production, whose distribution in $|\cos\theta^*|$ is intermediate between those expected for $J^P = 0^+$ and $J^P = 2^+$ states produced in gluon fusion. Two observables, $|\cos\theta^*|$ and $m_{\gamma\gamma}$, are used in the fit to data: $m_{\gamma\gamma}$ provides better separation power between the signal and the background, and $|\cos\theta^*|$ is sensitive to the spin.

The selected events contain two isolated photon candidates, as described in Ref. [18], but with the important difference that the kinematic requirements on the transverse momenta of the photons are proportional to $m_{\gamma\gamma}$. This choice reduces the correlation between $m_{\gamma\gamma}$ and $|\cos\theta^*|$ for the background to a negligible level. The selection requirements are set to $p_T^{\gamma 1} > 0.35m_{\gamma\gamma}$ and $p_T^{\gamma 2} > 0.25m_{\gamma\gamma}$. The fitted mass range is chosen to be $105 \text{ GeV} < m_{\gamma\gamma} < 160 \text{ GeV}$.

The intrinsic width of the resonance is assumed to be negligible compared to the detector resolution for both spin hypotheses. For this reason, the same probability density function is used to model the reconstructed mass spectra of both signal hypotheses, independent of the value of $|\cos\theta^*|$. The chosen function is the sum of a Crystal Ball [28] component, accounting for about 95% of the signal events, and a wider Gaussian component to model outlying events, as described in Ref. [18].

The $|\cos\theta^*|$ distributions of the signal, for either spin state, are obtained from simulated samples. The signal yields per $|\cos\theta^*|$ bin for a spin-0 particle are corrected for interference effects with the non-resonant diphoton background $gg \rightarrow \gamma\gamma$ [29]. The size of the correction is non-negligible only at high values of $|\cos\theta^*|$ and its value is taken as the systematic uncertainty on this effect. No interference between the spin-2 particle and the diphoton continuum background is assumed, since there are no theoretical models that describe it.

For the spin-2 state, the full size of the correction to the generated p_T spectrum of the diphoton system, described in Section 2, is taken as a systematic uncertainty.

The background distributions are derived directly from the observed data, using the two mass sidebands $105 \text{ GeV} < m_{\gamma\gamma} < 122 \text{ GeV}$ and $130 \text{ GeV} < m_{\gamma\gamma} < 160 \text{ GeV}$, where the signal contribution is negligible. The background shape as a function of $m_{\gamma\gamma}$ is modelled by a fifth-order polynomial with coefficients fitted to the data. The background shape as a function of $|\cos\theta^*|$ is taken from the two mass sidebands, since the remaining correlation between the two observables is small. The statistical uncertainties affecting the determination of the $|\cos\theta^*|$ distribution from the sidebands are propagated into the signal region (SR), $122 \text{ GeV} < m_{\gamma\gamma} < 130 \text{ GeV}$, independently for each $|\cos\theta^*|$ bin. Detailed studies of the data in the sidebands, reported in [19], show that possible residual correlations between $m_{\gamma\gamma}$ and $|\cos\theta^*|$ are not significant compared to the statistical uncertainties. A study of the background, based on a large sample of simulated events using the SHERPA generator [30], indicates the presence of a residual correlation at the level of 0.6% for $|\cos\theta^*| < 0.8$ and 2% elsewhere. These values are treated as the systematic uncertainties due to possible correlations between $m_{\gamma\gamma}$ and $|\cos\theta^*|$.

The fit to data is carried out simultaneously in the signal region and the two sideband regions. In the signal region, the likelihood is a function of the two discriminant variables $m_{\gamma\gamma}$ and $|\cos\theta^*|$, while in the sidebands only $m_{\gamma\gamma}$ is considered.

The number of data events selected in the signal region is 14977, compared with a background estimate of about 14300 events and an expected SM Higgs boson signal of about 370 events. Fig. 1 displays the data distribution for $|\cos\theta^*|$ in the signal region, overlaid with the signal and background components, fitted under the $J^P = 0^+$ hypothesis.

The likelihood function is fitted to data for both the spin-0 and spin-2 hypotheses with the signal and background normalisations treated as nuisance parameters. Fig. 2 shows the $|\cos\theta^*|$ distributions in the signal region, obtained after subtracting the estimated background, and compared with the expected distributions for spin-0 and spin-2 signals. The data points differ slightly between the two spin hypotheses, because the fitted background depends on the profiling of the nuisance parameters associated with the bin-by-bin systematic uncertainties.

5. $H \rightarrow ZZ^* \rightarrow 4\ell$ analysis

The $H \rightarrow ZZ^* \rightarrow 4\ell$ channel, where $\ell = e$ or μ , benefits from the presence of several observables dependent on spin and parity thanks to the full reconstruction of the four-lepton final state.

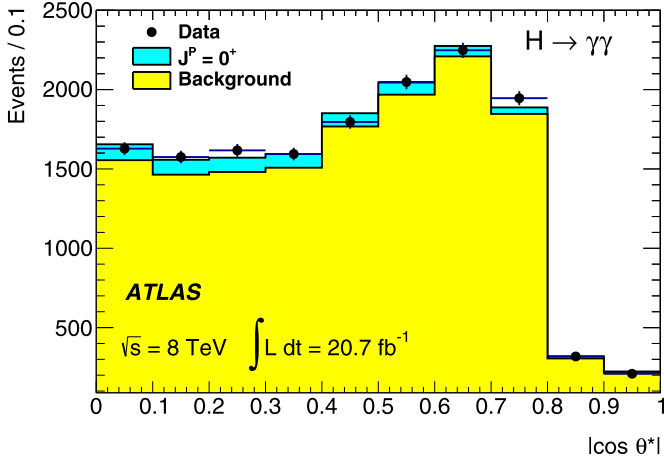
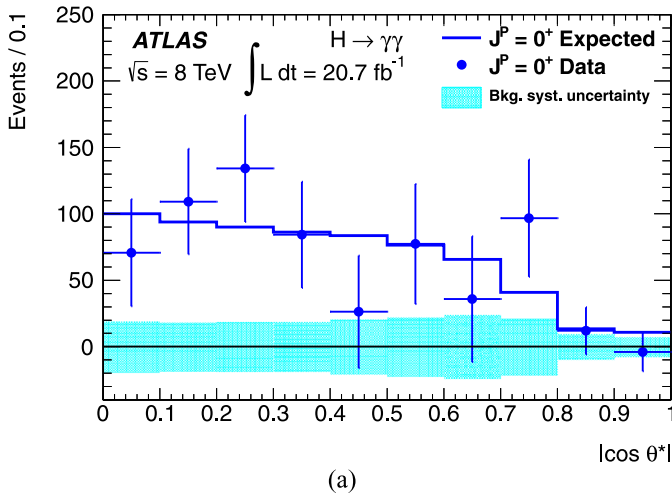
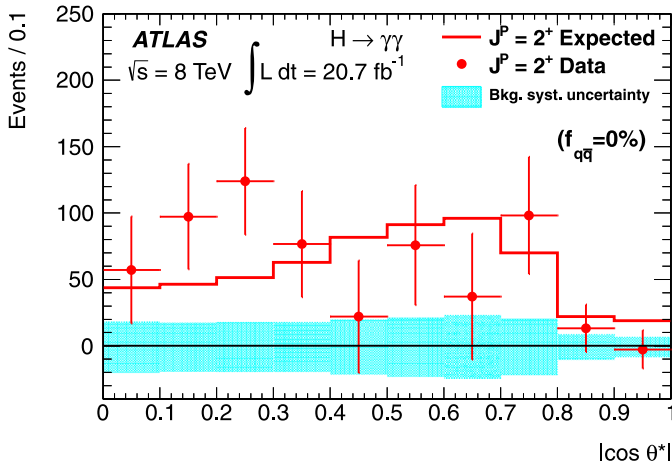


Fig. 1. Distribution of $|\cos\theta^*|$ for events in the signal region defined by $122 \text{ GeV} < m_{\gamma\gamma} < 130 \text{ GeV}$. The data (dots) are overlaid with the projection of the signal (blue/dark band) and background (yellow/light histogram) components obtained from the inclusive fit of the data under the spin-0 hypothesis.



(a)



(b)

Fig. 2. Distributions of background-subtracted data in the signal region as a function of $|\cos\theta^*|$. The expected distributions for (a) spin-0 and (b) spin-2 signals produced by gluon fusion, normalised to the fitted number of signal events, are overlaid as solid lines. The cyan/grey bands around the horizontal lines at zero show the systematic uncertainties on the background modelling before the fits, which include the statistical uncertainties on the data sidebands.

The kinematic observables are the reconstructed masses of the two Z boson candidates and the five production and decay angles described in the following. The Z boson candidates are denoted hereafter as Z_1 and Z_2 , where the index 1 refers to the lepton pair with the invariant mass closer to the central value of 91.1876 GeV of the Z boson mass [31]. Their respective masses are defined as m_{12} and m_{34} . The full definition of the production and decay angles as well as the description of their variation for different spin and parity values can be found in Ref. [20]. Here only a brief summary is given: θ_1 (θ_2) is the angle between the negatively charged final-state lepton in the Z_1 (Z_2) rest frame and the direction of flight of the Z_1 (Z_2) boson in the four-lepton rest frame. Φ is the angle between the decay planes defined by the two lepton pairs coming from the Z decays in the four-lepton rest frame. Φ_1 is the angle between the decay plane of the leading lepton pair and a plane defined by the momentum of the Z_1 in the four-lepton rest frame and the direction of the beam axis. θ^* is the production angle of the Z_1 defined in the four-lepton rest frame.

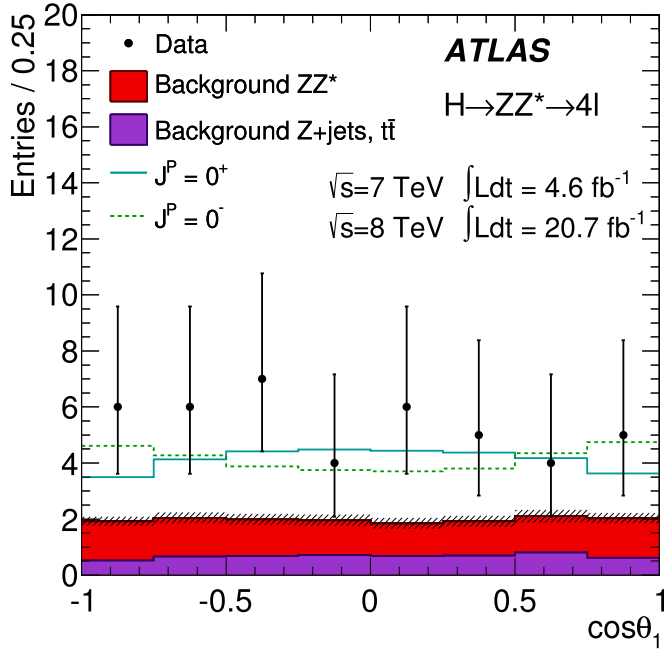
The lepton identification criteria and the analysis requirements follow the inclusive event selection described in Ref. [18]. To increase the sensitivity to the Higgs boson signal the final states are classified depending on the flavours of the lepton pairs. The events to reconstruct the variables sensitive to the spin and parity of the resonance are selected in the region of reconstructed four-lepton invariant mass $115 \text{ GeV} < m_{4\ell} < 130 \text{ GeV}$, defined as the signal mass window.

After the analysis requirements 43 candidate events are selected in data in the signal mass window, compared with an expected background of about 16 events, dominated by the continuum ZZ^* process, and about 18 signal events for a SM Higgs boson with a mass of 125.5 GeV . The irreducible ZZ^* background is estimated from Monte Carlo simulation, normalised to NLO calculations, while the reducible $t\bar{t}$, $Zb\bar{b}$ and Z + jets backgrounds are estimated from corresponding control regions in data, as described in Ref. [18]. Fig. 3 shows the $\cos(\theta_1)$ and m_{34} distributions for events passing the full selection in the signal mass window.

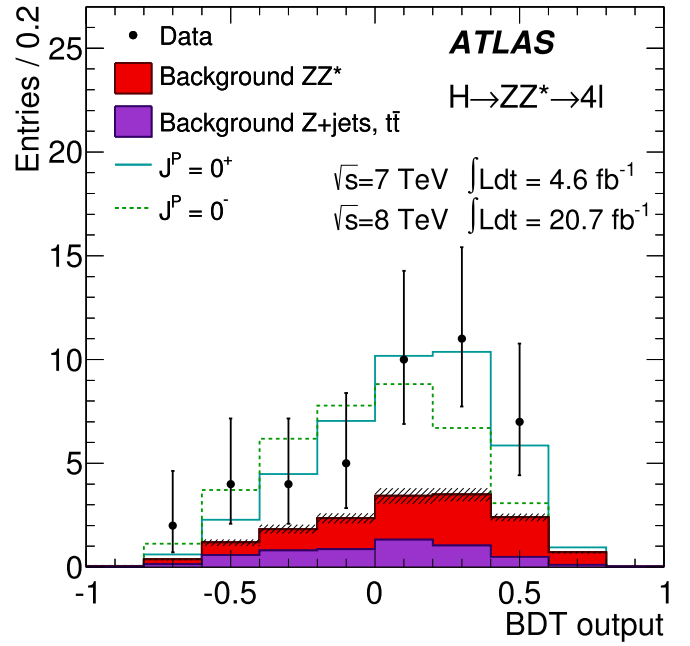
In order to distinguish between pairs of spin and parity states, the reconstructed observables described above, namely the five angles and the two invariant masses, are combined using a multivariate discriminant based on a boosted decision tree (BDT) [32]. The BDT is trained on simulated signal events after full reconstruction and event selection. Dedicated discriminants are defined for the separation between the Standard Model $J^P = 0^+$ hypothesis and each of the considered alternative models, $J^P = 0^-, 1^+, 1^-, 2^+$. In the case of the spin-2 hypothesis, the studies are performed as a function of the $q\bar{q}$ production fraction, $f_{q\bar{q}}$.

The response of the BDT classifiers is evaluated separately for each pair of signal hypotheses, including the expected backgrounds from other SM processes. In addition, to improve the overall sensitivity, the BDT responses are evaluated separately for two $m_{4\ell}$ regions with high and low signal-over-background ratio (S/B): low (115 – 121 GeV and 127 – 130 GeV) and high (121 – 127 GeV).

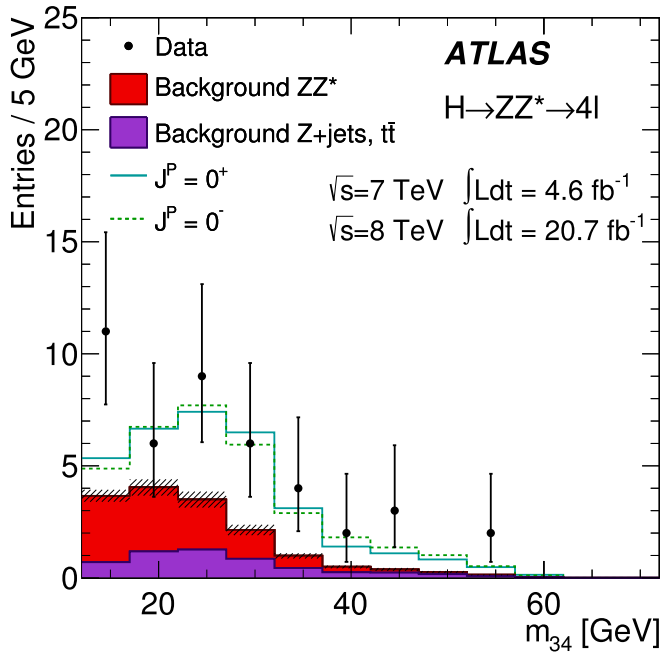
Systematic uncertainties on the shapes of the BDT output and on the normalisations of the high and low S/B mass regions are considered. These are due to uncertainties on the lepton identification efficiencies, the lepton energy scale and its resolution. A systematic uncertainty of $\pm 10\%$ on the normalisation of the high and low S/B mass regions is applied to take into account the experimental uncertainty on the mass of the Higgs boson. The systematic uncertainties on the overall background yields and on the integrated luminosity are treated as described in Ref. [18]. Fig. 4 shows the BDT discriminant distributions for the $J^P = 0^+$ versus $J^P = 0^-$



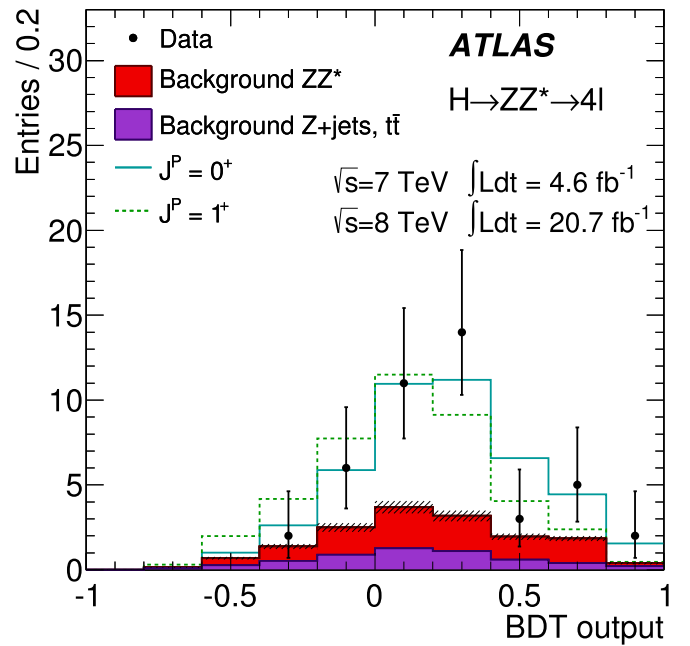
(a)



(a)



(b)



(b)

Fig. 3. Distributions of (a) $\cos(\theta_1)$ and (b) m_{34} for events passing the full selection in the signal mass window $115 \text{ GeV} < m_{4\ell} < 130 \text{ GeV}$ for the combined $\sqrt{s} = 7 \text{ TeV}$ and $\sqrt{s} = 8 \text{ TeV}$ datasets. The expected contributions from the $J^P = 0^+$ (solid line) and $J^P = 0^-$ (dashed line) signal hypotheses, and the irreducible ZZ^* background are shown, together with the measured contribution from reducible non- ZZ^* backgrounds. The hatched areas represent the uncertainty on the background yields from statistical, experimental, and theoretical sources.

Fig. 4. Distributions of the BDT output for data (points with error bars) and expectations based on MC simulation (histograms). The distribution of each discriminant is shown for a pair of spin and parity hypotheses for the signal: $J^P = 0^+$ (solid line) and $J^P = 0^-$ (dashed line) in (a), $J^P = 0^+$ (solid line) and $J^P = 1^+$ (dashed line) in (b). The signal contribution for each of the two hypotheses is scaled using the profiled value of the signal strength. The hatched areas represent the uncertainty on the background yields from statistical, experimental, and theoretical sources.

and the $J^P = 0^+$ versus $J^P = 1^+$ hypotheses. The distribution of the BDT output is used as a discriminant observable in the likelihood defined in Section 3.

In addition to the BDT analysis an alternative approach based on the differential decay rate with respect to the angles and the

masses, m_{12} and m_{34} , was also studied. These variables, corrected for detector acceptance and analysis selection effects, are used to construct a matrix-element-based discriminant. This alternative analysis yields results compatible with those obtained with the BDT, as described in detail in Ref. [20].

6. $H \rightarrow WW^* \rightarrow \ell\nu\ell\nu$ analysis

The analysis of the spin and parity in the $H \rightarrow WW^* \rightarrow \ell\nu\ell\nu$ channel is restricted to events containing two leptons of different flavour (one electron and one muon) and no observed jets with $p_T > 25$ GeV within $|\eta| < 2.5$ or with $p_T > 30$ GeV within $2.5 < |\eta| < 4.5$. The leading lepton is required to have $p_T > 25$ GeV and the sub-leading lepton $p_T > 15$ GeV. At least one of the two selected leptons is required to match a lepton that triggered the recording of the event.

The major sources of background after the dilepton selection are: $Z/\gamma^* + \text{jets}$, diboson ($WW, WZ/\gamma^*, ZZ/\gamma^*$), top-quark ($t\bar{t}$ and single top) production, and W bosons produced in association with hadronic jets where a jet is misidentified as a lepton. The WW background also includes the small fraction of dibosons produced via gluon fusion. The requirement of two high- p_T isolated leptons significantly reduces the background contributions from fake leptons. Multi-jet and Z/γ^* events are suppressed by requiring relative missing transverse momentum² $E_{T,\text{rel}}^{\text{miss}}$ above 20 GeV.

Further lepton topological requirements are applied to optimise the sensitivity for the separation of different spin hypotheses, namely requirements on the dilepton invariant mass $m_{\ell\ell} < 80$ GeV, the transverse momentum of the dilepton system $p_T^{\ell\ell} > 20$ GeV and the azimuthal angular difference between leptons $\Delta\phi_{\ell\ell} < 2.8$ rad. This selection, which significantly reduces the WW continuum and Z/γ^* backgrounds, defines the signal region (SR).

The contributions from WW , top-quark and $Z + \text{jets}$ processes predicted by MC simulation are normalised to observed rates in control regions (CRs) dominated by the relevant background sources. The $Z + \text{jets}$ CR is defined by inverting the $\Delta\phi_{\ell\ell}$ requirement and removing the $p_T^{\ell\ell}$ one. The $Z + \text{jets}$ normalisation factor of 0.92 with a total uncertainty of $\pm 8\%$ is derived from this control region and applied to the simulated sample. The WW CR is defined using the same selection as for the SR except that the $\Delta\phi_{\ell\ell}$ requirement is removed and the $m_{\ell\ell}$ requirement is inverted. The resulting WW normalisation factor applied to the MC prediction is 1.08 with a total uncertainty of $\pm 10\%$. The top-quark background is estimated as described in Ref. [18]. The ratio of the resulting prediction to the one from simulation alone is 1.07 with a total uncertainty of $\pm 14\%$. The $W + \text{jets}$ background is estimated entirely from data. The shapes and normalisations of non- WW diboson backgrounds are estimated using simulation and cross-checked in a validation region [18]. The correlations introduced among the different background sources by the presence of other processes in the control regions are fully included in the statistical procedure to test the compatibility between data and the two spin hypotheses, as described in Section 3.

After the selection, the data SR contains 3615 events, with 170 events expected from the SM Higgs boson signal and about 3300 events from background processes, after their normalisation to data in the CRs.

Spin correlations between the decay products affect the $H \rightarrow WW^* \rightarrow \ell\nu\ell\nu$ event topologies by shaping the angular distributions of the leptons as well as the distributions of the lepton momenta and missing transverse energy. Due to the presence of two neutrinos in the event, a direct calculation of the various decay angles is not possible. Two of the most sensitive variables for measuring the spin of the Higgs boson are the dilepton invariant mass, $m_{\ell\ell}$, and the azimuthal separation of the two leptons, $\Delta\phi_{\ell\ell}$. Fig. 5

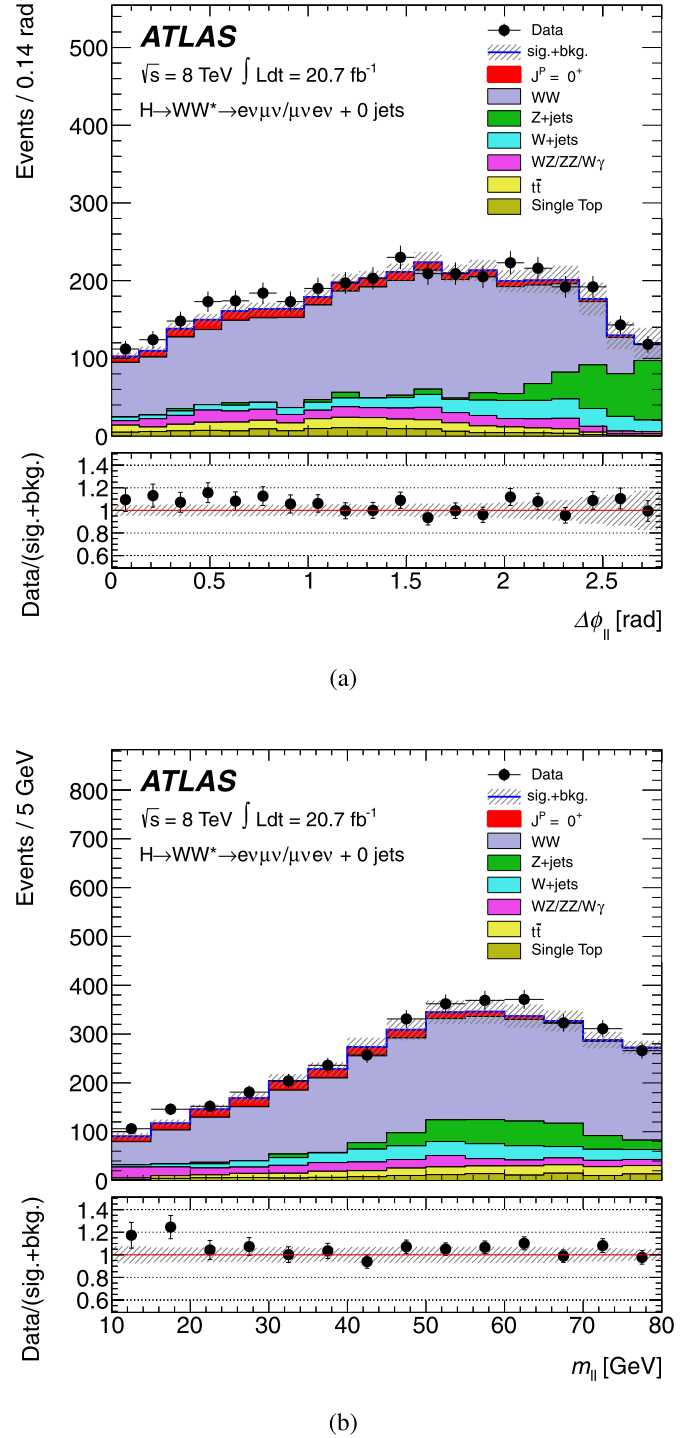


Fig. 5. Distributions of (a) $\Delta\phi_{\ell\ell}$ and (b) $m_{\ell\ell}$ in the signal region for $m_H = 125$ GeV and the $J^P = 0^+$ hypothesis. The signal is normalised to its SM expectation. In the lower part of the figures the ratio between data and the sum of signal and background is shown. The hatched areas represent the uncertainty on the signal and background yields from statistical, experimental, and theoretical sources.

shows the distributions of both variables in the signal region. The distributions observed in the data agree well with the MC prediction for the expected SM $J^P = 0^+$ signal. The dilepton transverse momentum, $p_T^{\ell\ell}$, also has sensitivity to different spin hypotheses.

A BDT algorithm is used to distinguish between the spin hypotheses. In addition to the three variables mentioned above, the transverse mass of the dilepton and missing momentum system,

² $E_{T,\text{rel}}^{\text{miss}} \equiv E_T^{\text{miss}} \cdot \sin \Delta\phi$, where $\Delta\phi$ is the azimuthal separation between the missing transverse momentum and the nearest reconstructed object (lepton or jet with $p_T > 25$ GeV) or $\pi/2$, whichever is smaller. The missing transverse energy E_T^{miss} is defined as the modulus of the missing transverse momentum.

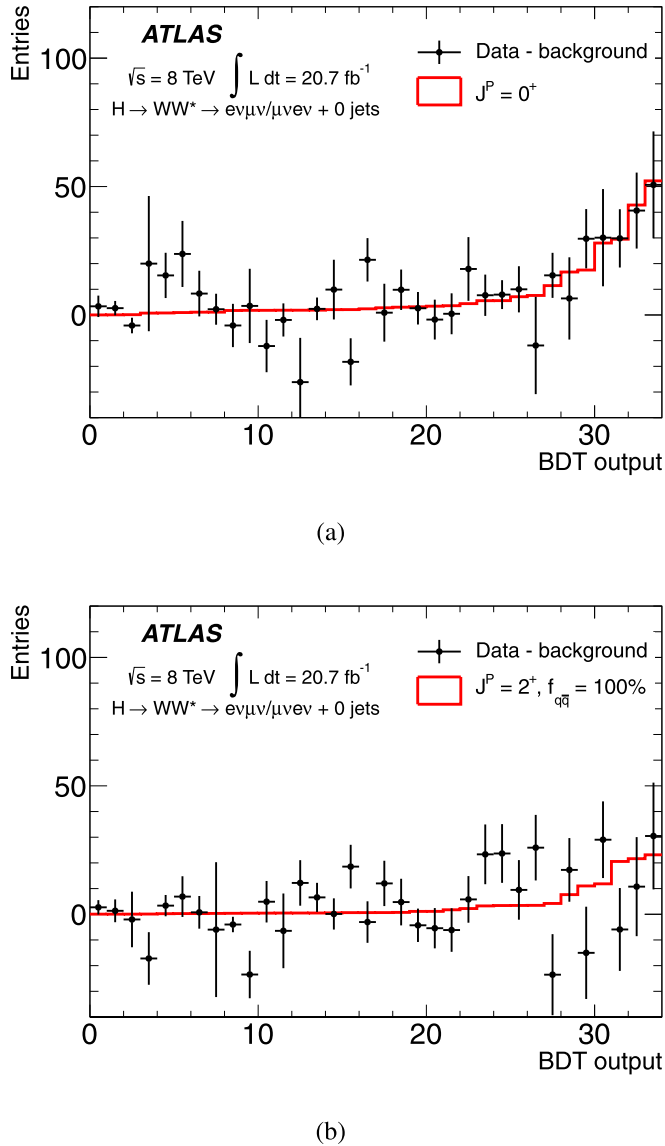


Fig. 6. One-dimensional distributions of the outputs of the BDT for the $H \rightarrow WW^*$ channel after background subtraction, using best-fit values for (a) $J^P = 0^+$ and (b) $J^P = 2^+$ with $f_{q\bar{q}} = 100\%$ hypotheses. In each case, the two-dimensional distribution of the two classifiers is remapped into a one-dimensional distribution, with the bins reordered in increasing number of expected signal events. Empty bins, defined as bins with expected content below 0.1, are removed.

m_T [18], is used in the BDT training as it provides a good separation between backgrounds and signals as well as some separation between the different spin hypotheses for the signals. Two separate BDT classifiers are developed for each hypothesis test: one classifier is trained to distinguish the $J^P = 0^+$ signal from the sum of all backgrounds while the second classifier separates the alternative spin-parity hypothesis ($J^P = 2^+, 1^+$ or 1^-) from the sum of all backgrounds. Background processes used to train both classifiers include WW , $t\bar{t}$ and single top, as well as WZ , ZZ , $W\gamma$, $W\gamma^*$, W + jets and Z + jets.

The resulting two-dimensional distribution of the two classifiers is then used in binned likelihood fits to test the data for compatibility with the presence of a $J^P = 0^+, 1^+, 1^-$ or 2^+ particle in the data. The analysis of $J^P = 2^+$, including the retraining of the second classifier with the $J^P = 2^+$ sample as signal, is repeated for each of the five values of $f_{q\bar{q}}$. The BDT output distributions

for data, after background subtraction, are shown in Fig. 6, after remapping the two-dimensional distribution of the two classifiers into a one-dimensional distribution.

The BDT relies on a good description of the input variables and their correlations. These were studied in detail and found to be well described by simulation [21]. In addition, dedicated studies were performed to verify that a BDT with the chosen four input variables is able to reliably separate the main backgrounds in a background-enriched region, and that the response is well modelled.

Two different categories of systematic uncertainties are considered: experimental or detector sources, such as the jet energy scale and resolution, or the lepton identification efficiencies, scale and resolution, as well as theoretical sources such as the estimation of the effect of higher-order contributions through variations of the QCD renormalisation and factorisation scales in the Monte Carlo simulation. The experimental uncertainties affect both the signal and background yields and are described in Ref. [18]. Monte Carlo samples with systematically varied parameters were analysed. Both the overall normalisation and shape distortions are included as nuisance parameters in the likelihood.

The WW background in the signal region is evaluated through extrapolation from a control region using the simulation. The theoretical uncertainties on the extrapolation parameter $\alpha = N_{SR}/N_{CR}$, the ratio of the number of events passing the signal region selection to the number passing the control region selection, are evaluated according to the prescription of Ref. [33]. Several sources of uncertainty on the normalisation are considered: uncertainties on the QCD renormalisation and factorisation scales, Parton Density Functions (PDF), the choice of Monte Carlo generator, and the underlying event and parton shower model. The total uncertainty on the extrapolation is $\pm 4.8\%$. Another important uncertainty arises from the shape modelling of the irreducible WW continuum background. The uncertainty on the shapes of the BDT discriminants is studied by varying the factorisation and renormalisation scales, by comparing the predictions of HERWIG [34] and PYTHIA8 leading-order parton shower programs, and by evaluating the uncertainties from the CT10 [35] PDF error set and combining them with the difference in central values between NNPDF [36] and CT10. An envelope for the predicted BDT shape for each discriminant is derived and included in the binned likelihood fit as a shape uncertainty.

7. Results

The SM $J^P = 0^+$ hypothesis is tested against several alternative spin-parity hypotheses using the analyses described in the previous sections. Using the statistical procedure described in Section 3, integral probabilities, the p_0 -values, are determined to quantify the level of agreement of the data with different spin-parity hypotheses. When giving the confidence level associated with the rejection of a spin-parity hypothesis, the CL_s approach defined in Eq. (3) is used.

7.1. Systematic uncertainties

The sources of systematic uncertainty accounted for in the analyses of the individual channels are discussed in Sections 4, 5 and 6. In the combination, the correlations among the common sources of systematic uncertainties across channels are taken into account. Systematic uncertainties on electron and muon identification, reconstruction and trigger efficiencies, as well as on their energy and momentum resolution, are common to both the $H \rightarrow ZZ^*$ and $H \rightarrow WW^*$ channels. Systematic uncertainties on the energy scale of electrons and photons affect all three decay channels. It was also verified that the results presented in the following are insen-

sitive to variations of the Higgs boson mass within the measured accuracy of about ± 0.6 GeV [18].

The overall impact of the systematic uncertainties is evaluated by comparing the baseline results of the likelihood fits obtained by profiling all nuisance parameters not directly measured from the data, with the results obtained by fixing them at their nominal values. For all tested hypotheses, the combined rejection significance is found to be degraded by less than 0.3σ when including all nuisance parameters in the fit with respect to fixing them at their nominal values.

The production mode has a significant impact on the underlying p_T spectrum of the Higgs boson. For signals produced through gluon fusion, the dependence on the p_T modelling was studied by comparing the discriminant observables before and after re-weighting the signal to the POWHEG+PYTHIA8 spectrum. However, the impact on the discriminant observables is found to be negligible compared to other sources of systematic uncertainty and therefore is neglected. For the $q\bar{q}$ -initiated processes the p_T spectrum is expected to be softer than for processes produced via gluon fusion. Since no higher-order QCD predictions are available for the $q\bar{q}$ annihilation production process, no specific systematic uncertainty is assigned to the p_T spectrum of such signals. The impact of the large variation obtained by re-weighting the signals produced at leading order in $q\bar{q}$ annihilation for the $J^P = 2^+$ model to the POWHEG+PYTHIA8 gluon-fusion prediction was evaluated. The resulting weights increase from about unity at low transverse momentum to about four near 100 GeV. The $H \rightarrow WW^*$ and $H \rightarrow ZZ^*$ channels are almost insensitive to such re-weighting, which leads to changes in the BDT discriminant shapes of the order of a few percent. The $H \rightarrow \gamma\gamma$ channel is more sensitive to the signal p_T spectrum due to the impact on its acceptance at high $|\cos\theta^*|$ values. For this channel, the expected sensitivity for the spin-2 rejection is reduced by about 30% for $f_{q\bar{q}} = 100\%$, when the re-weighting is applied. Since the combined result for this case is dominated by the $H \rightarrow ZZ^*$ and $H \rightarrow WW^*$ channels, the overall impact of this re-weighting on the combined $J^P = 2^+$ rejection is negligible, below 0.1σ .

7.2. Test of SM $J^P = 0^+$ against $J^P = 0^-$

The distributions of the test statistics q from the $H \rightarrow ZZ^*$ channel for the $J^P = 0^+$ and 0^- hypotheses are shown in Fig. 7 together with the observed value.

The expected and observed rejections of the $J^P = 0^+$ and 0^- hypotheses are summarised in Table 1. The data are in agreement with the $J^P = 0^+$ hypothesis, while the 0^- hypothesis is excluded at 97.8% CL.

7.3. Test of SM $J^P = 0^+$ against $J^P = 1^+$

The expected and observed rejections of the $J^P = 0^+$ and 1^+ hypotheses in the $H \rightarrow ZZ^*$ and $H \rightarrow WW^*$ channels and their combination are summarised in Table 2. For both channels, the results are in agreement with the $J^P = 0^+$ hypothesis. In the $H \rightarrow ZZ^*$ channel, the 1^+ hypothesis is excluded at 99.8% CL, while in the $H \rightarrow WW^*$ channel, it is excluded at 92% CL. The combination excludes this hypothesis at 99.97% CL.

7.4. Test of SM $J^P = 0^+$ against $J^P = 1^-$

The expected and observed rejections of the $J^P = 0^+$ and 1^- hypotheses in the $H \rightarrow ZZ^*$ and $H \rightarrow WW^*$ channels and their combination are summarised in Table 3. For both channels, the results are in agreement with the $J^P = 0^+$ hypothesis. In the $H \rightarrow ZZ^*$ channel, the 1^- hypothesis is excluded

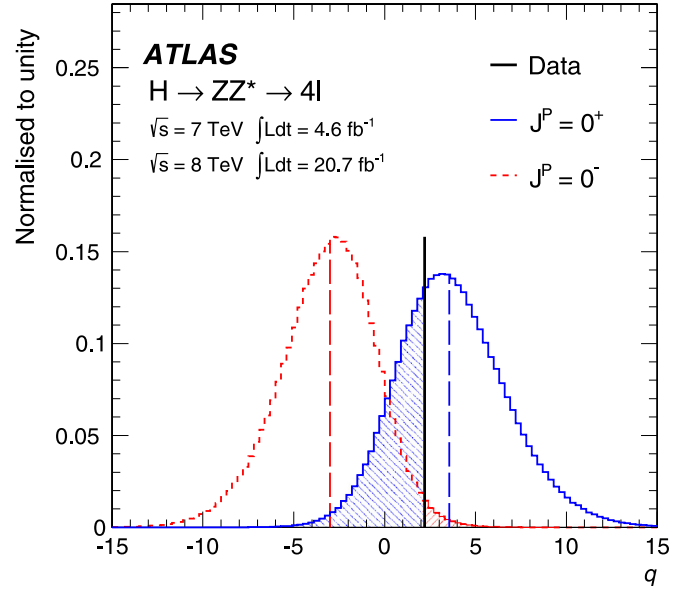


Fig. 7. Expected distributions of $q = \log(\mathcal{L}(J^P = 0^+)/\mathcal{L}(J^P = 0^-))$, the logarithm of the ratio of profiled likelihoods, under the $J^P = 0^+$ and 0^- hypotheses for the Standard Model $J^P = 0^+$ (blue/solid line distribution) or 0^- (red/dashed line distribution) signals. The observed value is indicated by the vertical solid line and the expected medians by the dashed lines. The coloured areas correspond to the integrals of the expected distributions up to the observed value and are used to compute the p_0 -values for the rejection of each hypothesis.

at 94% CL. In the $H \rightarrow WW^*$ channel, the 1^- hypothesis is excluded at 98% CL. The combination excludes this hypothesis at 99.7% CL.

7.5. Test of SM $J^P = 0^+$ against $J^P = 2^+$

The expected and observed rejections of the $J^P = 0^+$ and 2^+ hypotheses in the three channels are summarised in Table 4, for all $f_{q\bar{q}}$ values of the spin-2 particle considered. For all three channels, the results are in agreement with the spin-0 hypothesis. The results from the $H \rightarrow \gamma\gamma$ channel exclude a spin-2 particle produced via gluon fusion ($f_{q\bar{q}} = 0$) at 99.3% CL. The separation between the two spin hypotheses in this channel decreases with increasing $f_{q\bar{q}}$. For large values of $f_{q\bar{q}}$, the $|\cos\theta^*|$ distributions associated with the spin-0 and spin-2 signals become very similar. In the case of the $H \rightarrow ZZ^*$ channel, a separation slightly above one standard deviation is expected between the $J^P = 0^+$ and $J^P = 2^+$ hypotheses, with little dependence on the production mechanism. The $H \rightarrow WW^*$ channel has the opposite behaviour to the $H \rightarrow \gamma\gamma$ one, with the best expected rejection achieved for large values of $f_{q\bar{q}}$, as illustrated in Table 4. The results for the $H \rightarrow WW^*$ channel are also in agreement with the $J^P = 0^+$ hypothesis. The $J^P = 2^+$ hypothesis is excluded with a CL above 95%. The data are in better agreement with the $J^P = 0^+$ hypothesis over the full range of $f_{q\bar{q}}$.

Table 5 shows the expected and observed p_0 -values for both the $J^P = 0^+$ and $J^P = 2^+$ hypotheses for the combination of the $H \rightarrow \gamma\gamma$, $H \rightarrow ZZ^*$ and $H \rightarrow WW^*$ channels. The test statistics calculated on data are compared to the corresponding expectations obtained from pseudo-experiments, as a function of $f_{q\bar{q}}$. The data are in good agreement with the Standard Model $J^P = 0^+$ hypothesis over the full $f_{q\bar{q}}$ range. Fig. 8 shows the comparison of the expected and observed CL_s values for the $J^P = 2^+$ rejection as a function of $f_{q\bar{q}}$. The observed exclusion of the $J^P = 2^+$ hypothesis in favour of the Standard Model $J^P = 0^+$ hypothesis exceeds 99.9% CL for all values of $f_{q\bar{q}}$.

Table 1
Summary of results for the 0^+ versus 0^- test in the $H \rightarrow ZZ^*$ channel. The expected p_0 -values for rejecting the 0^+ and 0^- hypotheses (assuming the alternative hypothesis) are shown in the second and third columns. The fourth and fifth columns show the observed p_0 -values, while the CL_s value for excluding the 0^- hypothesis is given in the last column.

Channel	0^- assumed Exp. $p_0(J^P = 0^+)$	0^+ assumed Exp. $p_0(J^P = 0^-)$	Obs. $p_0(J^P = 0^+)$	Obs. $p_0(J^P = 0^-)$	$CL_s(J^P = 0^-)$
$H \rightarrow ZZ^*$	$1.5 \cdot 10^{-3}$	$3.7 \cdot 10^{-3}$	0.31	0.015	0.022

Table 2
Summary of results for the $J^P = 0^+$ versus 1^+ test in the $H \rightarrow ZZ^*$ and $H \rightarrow WW^*$ channels, as well as their combination. The expected p_0 -values for rejecting the $J^P = 0^+$ and 1^+ hypotheses (assuming the alternative hypothesis) are shown in the second and third columns. The fourth and fifth columns show the observed p_0 -values, while the CL_s values for excluding the 1^+ hypothesis are given in the last column.

Channel	1^+ assumed Exp. $p_0(J^P = 0^+)$	0^+ assumed Exp. $p_0(J^P = 1^+)$	Obs. $p_0(J^P = 0^+)$	Obs. $p_0(J^P = 1^+)$	$CL_s(J^P = 1^+)$
$H \rightarrow ZZ^*$	$4.6 \cdot 10^{-3}$	$1.6 \cdot 10^{-3}$	0.55	$1.0 \cdot 10^{-3}$	$2.0 \cdot 10^{-3}$
$H \rightarrow WW^*$	0.11	0.08	0.70	0.02	0.08
Combination	$2.7 \cdot 10^{-3}$	$4.7 \cdot 10^{-4}$	0.62	$1.2 \cdot 10^{-4}$	$3.0 \cdot 10^{-4}$

Table 3
Summary of results for the $J^P = 0^+$ versus 1^- test in the $H \rightarrow ZZ^*$ and $H \rightarrow WW^*$ channels, as well as their combination. The expected p_0 -values for rejecting the $J^P = 0^+$ and 1^- hypotheses (assuming the alternative hypothesis) are shown in the second and third columns. The fourth and fifth columns show the observed p_0 -values, while the CL_s values for excluding the 1^- hypothesis are given in the last column.

Channel	1^- assumed Exp. $p_0(J^P = 0^+)$	0^+ assumed Exp. $p_0(J^P = 1^-)$	Obs. $p_0(J^P = 0^+)$	Obs. $p_0(J^P = 1^-)$	$CL_s(J^P = 1^-)$
$H \rightarrow ZZ^*$	$0.9 \cdot 10^{-3}$	$3.8 \cdot 10^{-3}$	0.15	0.051	0.060
$H \rightarrow WW^*$	0.06	0.02	0.66	0.006	0.017
Combination	$1.4 \cdot 10^{-3}$	$3.6 \cdot 10^{-4}$	0.33	$1.8 \cdot 10^{-3}$	$2.7 \cdot 10^{-3}$

Table 4
Summary of results for the various fractions $f_{q\bar{q}}$ of the $q\bar{q}$ production of the spin-2 particle for the $H \rightarrow \gamma\gamma$ (top), $H \rightarrow ZZ^*$ (middle), and $H \rightarrow WW^*$ (bottom) channels. The expected p_0 -values for rejecting the $J^P = 0^+$ and $J^P = 2^+$ hypotheses (assuming the alternative hypothesis) are shown in the second and third columns. The fourth and fifth columns show the observed p_0 -values, while the CL_s values for excluding the $J^P = 2^+$ hypothesis are given in the last column.

$f_{q\bar{q}}$	2^+ assumed Exp. $p_0(J^P = 0^+)$	0^+ assumed Exp. $p_0(J^P = 2^+)$	Obs. $p_0(J^P = 0^+)$	Obs. $p_0(J^P = 2^+)$	$CL_s(J^P = 2^+)$
$H \rightarrow \gamma\gamma$					
100%	0.148	0.135	0.798	0.025	0.124
75%	0.319	0.305	0.902	0.033	0.337
50%	0.198	0.187	0.708	0.076	0.260
25%	0.052	0.039	0.609	0.021	0.054
0%	0.012	0.005	0.588	0.003	0.007
$H \rightarrow ZZ^*$					
100%	0.102	0.082	0.962	0.001	0.026
75%	0.117	0.099	0.923	0.003	0.039
50%	0.129	0.113	0.943	0.002	0.035
25%	0.125	0.107	0.944	0.002	0.036
0%	0.099	0.092	0.532	0.079	0.169
$H \rightarrow WW^*$					
100%	0.013	$3.6 \cdot 10^{-4}$	0.541	$1.7 \cdot 10^{-4}$	$3.6 \cdot 10^{-4}$
75%	0.028	0.003	0.586	0.001	0.003
50%	0.042	0.009	0.616	0.003	0.008
25%	0.048	0.019	0.622	0.008	0.020
0%	0.086	0.054	0.731	0.013	0.048

Table 5
Expected and observed p_0 -values for the $J^P = 0^+$ and $J^P = 2^+$ hypotheses as a function of the fraction $f_{q\bar{q}}$ of the $q\bar{q}$ spin-2 production mechanism. The values are tabulated for the combination of the $H \rightarrow \gamma\gamma$, $H \rightarrow ZZ^*$ and $H \rightarrow WW^*$ channels. The CL_s values for excluding the $J^P = 2^+$ hypothesis are given in the last column.

$f_{q\bar{q}}$	2^+ assumed Exp. $p_0(J^P = 0^+)$	0^+ assumed Exp. $p_0(J^P = 2^+)$	Obs. $p_0(J^P = 0^+)$	Obs. $p_0(J^P = 2^+)$	$CL_s(J^P = 2^+)$
100%	$3.0 \cdot 10^{-3}$	$8.8 \cdot 10^{-5}$	0.81	$1.6 \cdot 10^{-6}$	$0.8 \cdot 10^{-5}$
75%	$9.5 \cdot 10^{-3}$	$8.8 \cdot 10^{-4}$	0.81	$3.2 \cdot 10^{-5}$	$1.7 \cdot 10^{-4}$
50%	$1.3 \cdot 10^{-2}$	$2.7 \cdot 10^{-3}$	0.84	$8.6 \cdot 10^{-5}$	$5.3 \cdot 10^{-4}$
25%	$6.4 \cdot 10^{-3}$	$2.1 \cdot 10^{-3}$	0.80	$0.9 \cdot 10^{-4}$	$4.6 \cdot 10^{-4}$
0%	$2.1 \cdot 10^{-3}$	$5.5 \cdot 10^{-4}$	0.63	$1.5 \cdot 10^{-4}$	$4.2 \cdot 10^{-4}$

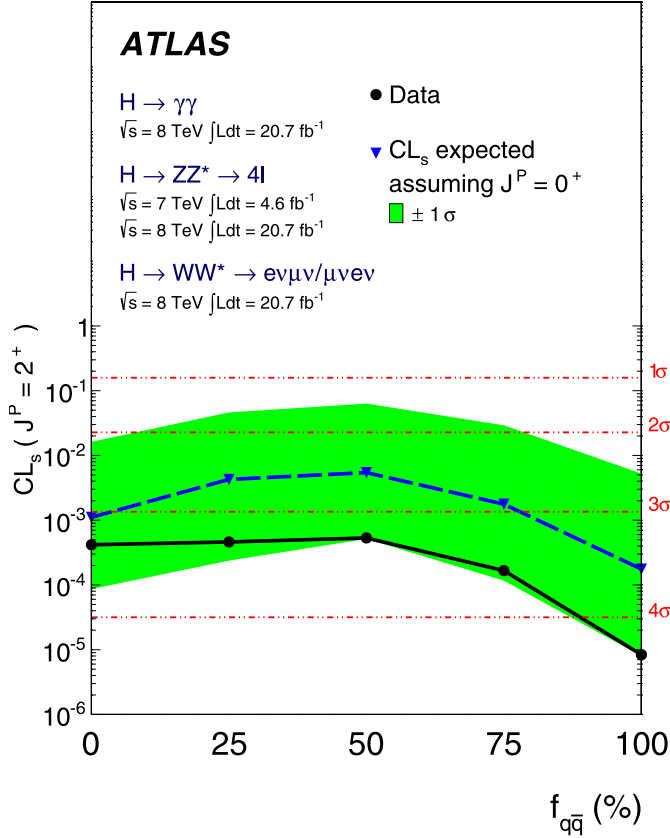


Fig. 8. Expected (blue triangles/dashed line) and observed (black circles/solid line) confidence levels, $CL_s(J^P = 2^+)$, of the $J^P = 2^+$ hypothesis as a function of the fraction $f_{q\bar{q}}$ (see text) for the spin-2 particle. The green bands represent the 68% expected exclusion range for a signal with assumed $J^P = 0^+$. On the right y-axis, the corresponding numbers of Gaussian standard deviations are given, using the one-sided convention.

7.6. Summary

The observed and expected CL_s values for the exclusion of the different spin–parity hypotheses are summarised in Fig. 9. For the spin-2 hypothesis, the CL_s value for the specific 2_m^+ model, discussed in Section 2, is displayed.

8. Conclusions

The Standard Model $J^P = 0^+$ hypothesis for the Higgs boson has been compared to alternative spin–parity hypotheses using $\sqrt{s} = 8$ TeV (20.7 fb^{-1}) and 7 TeV (4.6 fb^{-1}) proton–proton collision data collected by the ATLAS experiment at the LHC. The Higgs boson decays $H \rightarrow \gamma\gamma$, $H \rightarrow ZZ^* \rightarrow 4\ell$ and $H \rightarrow WW^* \rightarrow \ell\nu\ell\nu$ have been used to test several specific alternative models, including $J^P = 0^-, 1^+, 1^-$ and a graviton-inspired $J^P = 2^+$ model with minimal couplings to SM particles. The data favour the Standard Model quantum numbers of $J^P = 0^+$. The 0^- hypothesis is rejected at 97.8% CL by using the $H \rightarrow ZZ^* \rightarrow 4\ell$ decay alone. The 1^+ and 1^- hypotheses are rejected with a CL of at least 99.7% by combining the $H \rightarrow ZZ^* \rightarrow 4\ell$ and $H \rightarrow WW^* \rightarrow \ell\nu\ell\nu$ channels. Finally, the $J^P = 2^+$ model is rejected at more than 99.9% CL by combining all three bosonic channels, $H \rightarrow \gamma\gamma$, $H \rightarrow ZZ^* \rightarrow 4\ell$ and $H \rightarrow WW^* \rightarrow \ell\nu\ell\nu$, independent of the assumed admixture of gluon-fusion and quark–antiquark production. All alternative models studied in this Letter are excluded without assumptions on the strength of the couplings of the Higgs boson to SM parti-

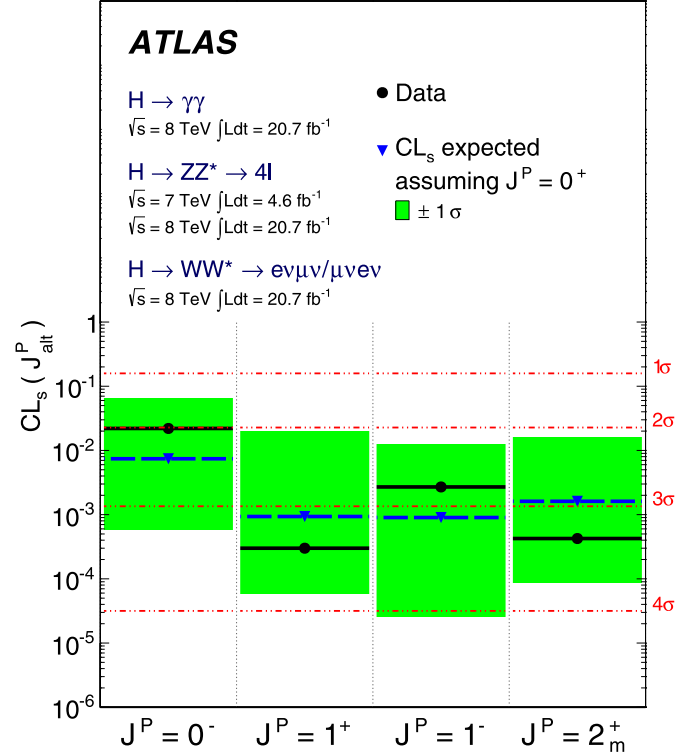


Fig. 9. Expected (blue triangles/dashed lines) and observed (black circles/solid lines) confidence level CL_s for alternative spin–parity hypotheses assuming a $J^P = 0^+$ signal. The green band represents the 68% $CL_s(J^P_{\text{alt}})$ expected exclusion range for a signal with assumed $J^P = 0^+$. For the spin-2 hypothesis, the results for the specific 2_m^+ model, discussed in Section 2, are shown. On the right y-axis, the corresponding numbers of Gaussian standard deviations are given, using the one-sided convention.

cles. These studies provide evidence for the spin-0 nature of the Higgs boson, with positive parity being strongly preferred.

Acknowledgements

We thank CERN for the very successful operation of the LHC, as well as the support staff from our institutions without whom ATLAS could not be operated efficiently.

We acknowledge the support of ANPCyT, Argentina; YerPhI, Armenia; ARC, Australia; BMWF and FWF, Austria; ANAS, Azerbaijan; SSTC, Belarus; CNPq and FAPESP, Brazil; NSERC, NRC and CFI, Canada; CERN; CONICYT, Chile; CAS, MOST and NSFC, China; COLCIENCIAS, Colombia; MSMT CR, MPO CR and VSC CR, Czech Republic; DNRF, DNSRC and Lundbeck Foundation, Denmark; EPLANET, ERC and NSRF, European Union; IN2P3-CNRS, CEA-DSM/IRFU, France; GNSF, Georgia; BMBF, DFG, HGF, MPG and AvH Foundation, Germany; GSRT and NSRF, Greece; ISF, MINERVA, GIF, DIP and Benoziyo Center, Israel; INFN, Italy; MEXT and JSPS, Japan; CNRST, Morocco; FOM and NWO, Netherlands; BRF and RCN, Norway; MNiSW, Poland; GRICES and FCT, Portugal; MERYS (MECTS), Romania; MES of Russia and ROSATOM, Russian Federation; JINR; MSTD, Serbia; MSSR, Slovakia; ARRS and MIZŠ, Slovenia; DST/NRF, South Africa; MICINN, Spain; SRC and Wallenberg Foundation, Sweden; SER, SNSF and Cantons of Bern and Geneva, Switzerland; NSC, Taiwan; TAEK, Turkey; STFC, the Royal Society and Leverhulme Trust, United Kingdom; DOE and NSF, United States of America.

The crucial computing support from all WLCG partners is acknowledged gratefully, in particular from CERN and the ATLAS Tier-1 facilities at TRIUMF (Canada), NDGF (Denmark, Norway, Sweden), CC-IN2P3 (France), KIT/GridKA (Germany), INFN-CNAF (Italy),

V. Büscher⁸², P. Bussey⁵³, C.P. Buszello¹⁶⁷, B. Butler⁵⁷, J.M. Butler²², C.M. Buttar⁵³,
 J.M. Butterworth⁷⁷, W. Buttinger²⁸, A. Buzatu⁵³, M. Byszewski¹⁰, S. Cabrera Urbán¹⁶⁸,
 D. Caforio^{20a,20b}, O. Cakir^{4a}, P. Calafiura¹⁵, G. Calderini⁷⁹, P. Calfayan⁹⁹, R. Calkins¹⁰⁷,
 L.P. Caloba^{24a}, R. Caloi^{133a,133b}, D. Calvet³⁴, S. Calvet³⁴, R. Camacho Toro⁴⁹,
 P. Camarri^{134a,134b}, D. Cameron¹¹⁸, L.M. Caminada¹⁵, R. Caminal Armadans¹²,
 S. Campana³⁰, M. Campanelli⁷⁷, V. Canale^{103a,103b}, F. Canelli³¹, A. Canepa^{160a},
 J. Cantero⁸¹, R. Cantrill⁷⁶, T. Cao⁴⁰, M.D.M. Capeans Garrido³⁰, I. Caprini^{26a},
 M. Caprini^{26a}, D. Capriotti¹⁰⁰, M. Capua^{37a,37b}, R. Caputo⁸², R. Cardarelli^{134a}, T. Carli³⁰,
 G. Carlino^{103a}, L. Carminati^{90a,90b}, S. Caron¹⁰⁵, E. Carquin^{32b}, G.D. Carrillo-Montoya^{146c},
 A.A. Carter⁷⁵, J.R. Carter²⁸, J. Carvalho^{125a,h}, D. Casadei⁷⁷, M.P. Casado¹², C. Caso^{50a,50b,*},
 E. Castaneda-Miranda^{146b}, A. Castelli¹⁰⁶, V. Castillo Gimenez¹⁶⁸, N.F. Castro^{125a},
 G. Cataldi^{72a}, P. Catastini⁵⁷, A. Catinaccio³⁰, J.R. Catmore³⁰, A. Cattai³⁰,
 G. Cattani^{134a,134b}, S. Caughron⁸⁹, V. Cavaliere¹⁶⁶, D. Cavalli^{90a}, M. Cavalli-Sforza¹²,
 V. Cavasinni^{123a,123b}, F. Ceradini^{135a,135b}, B. Cerio⁴⁵, A.S. Cerqueira^{24b}, A. Cerri¹⁵,
 L. Cerrito⁷⁵, F. Cerutti¹⁵, A. Cervelli¹⁷, S.A. Cetin^{19b}, A. Chafaq^{136a}, D. Chakraborty¹⁰⁷,
 I. Chalupkova¹²⁸, K. Chan³, P. Chang¹⁶⁶, B. Chapleau⁸⁶, J.D. Chapman²⁸, J.W. Chapman⁸⁸,
 D.G. Charlton¹⁸, V. Chavda⁸³, C.A. Chavez Barajas³⁰, S. Cheatham⁸⁶, S. Chekanov⁶,
 S.V. Chekulaev^{160a}, G.A. Chelkov⁶⁴, M.A. Chelstowska⁸⁸, C. Chen⁶³, H. Chen²⁵,
 S. Chen^{33c}, X. Chen¹⁷⁴, Y. Chen³⁵, Y. Cheng³¹, A. Cheplakov⁶⁴,
 R. Cherkaoui El Moursli^{136e}, V. Chernyatin^{25,*}, E. Cheu⁷, L. Chevalier¹³⁷, V. Chiarella⁴⁷,
 G. Chiefari^{103a,103b}, J.T. Childers³⁰, A. Chilingarov⁷¹, G. Chiodini^{72a}, A.S. Chisholm¹⁸,
 R.T. Chislett⁷⁷, A. Chitan^{26a}, M.V. Chizhov⁶⁴, G. Choudalakis³¹, S. Chouridou⁹,
 B.K.B. Chow⁹⁹, I.A. Christidi⁷⁷, A. Christov⁴⁸, D. Chromek-Burckhart³⁰, M.L. Chu¹⁵²,
 J. Chudoba¹²⁶, G. Ciapetti^{133a,133b}, A.K. Ciftci^{4a}, R. Ciftci^{4a}, D. Cinca⁶², V. Cindro⁷⁴,
 A. Ciochio¹⁵, M. Cirilli⁸⁸, P. Cirkovic^{13b}, Z.H. Citron¹⁷³, M. Citterio^{90a}, M. Ciubancan^{26a},
 A. Clark⁴⁹, P.J. Clark⁴⁶, R.N. Clarke¹⁵, J.C. Clemens⁸⁴, B. Clement⁵⁵, C. Clement^{147a,147b},
 Y. Coadou⁸⁴, M. Cobal^{165a,165c}, A. Coccaro¹³⁹, J. Cochran⁶³, S. Coelli^{90a}, L. Coffey²³,
 J.G. Cogan¹⁴⁴, J. Coggeshall¹⁶⁶, J. Colas⁵, B. Cole³⁵, S. Cole¹⁰⁷, A.P. Colijn¹⁰⁶,
 C. Collins-Tooth⁵³, J. Collot⁵⁵, T. Colombo^{58c}, G. Colon⁸⁵, G. Compostella¹⁰⁰,
 P. Conde Muiño^{125a}, E. Coniavitis¹⁶⁷, M.C. Conidi¹², S.M. Consonni^{90a,90b}, V. Consorti⁴⁸,
 S. Constantinescu^{26a}, C. Conta^{120a,120b}, G. Conti⁵⁷, F. Conventi^{103a,i}, M. Cooke¹⁵,
 B.D. Cooper⁷⁷, A.M. Cooper-Sarkar¹¹⁹, N.J. Cooper-Smith⁷⁶, K. Copic¹⁵, T. Cornelissen¹⁷⁶,
 M. Corradi^{20a}, F. Corriveau^{86,j}, A. Corso-Radu¹⁶⁴, A. Cortes-Gonzalez¹², G. Cortiana¹⁰⁰,
 G. Costa^{90a}, M.J. Costa¹⁶⁸, D. Costanzo¹⁴⁰, D. Côte⁸, G. Cottin^{32a}, L. Courneyea¹⁷⁰,
 G. Cowan⁷⁶, B.E. Cox⁸³, K. Cranmer¹⁰⁹, S. Crépe-Renaudin⁵⁵, F. Crescioli⁷⁹,
 M. Cristinziani²¹, G. Crosetti^{37a,37b}, C.-M. Cuciuc^{26a}, C. Cuenca Almenar¹⁷⁷,
 T. Cuhadar Donszelmann¹⁴⁰, J. Cummings¹⁷⁷, M. Curatolo⁴⁷, C. Cuthbert¹⁵¹, H. Czirr¹⁴²,
 P. Czodrowski⁴⁴, Z. Czyzula¹⁷⁷, S. D'Auria⁵³, M. D'Onofrio⁷³, A. D'Orazio^{133a,133b},
 M.J. Da Cunha Sargedas De Sousa^{125a}, C. Da Via⁸³, W. Dabrowski^{38a}, A. Dafinca¹¹⁹,
 T. Dai⁸⁸, F. Dallaire⁹⁴, C. Dallapiccola⁸⁵, M. Dam³⁶, D.S. Damiani¹³⁸, A.C. Daniells¹⁸,
 V. Dao¹⁰⁵, G. Darbo^{50a}, G.L. Darlea^{26c}, S. Darmora⁸, J.A. Dassoulas⁴², W. Davey²¹,
 C. David¹⁷⁰, T. Davidek¹²⁸, E. Davies^{119,d}, M. Davies⁹⁴, O. Davignon⁷⁹, A.R. Davison⁷⁷,
 Y. Davygora^{58a}, E. Dawe¹⁴³, I. Dawson¹⁴⁰, R.K. Daya-Ishmukhametova²³, K. De⁸,
 R. de Asmundis^{103a}, S. De Castro^{20a,20b}, S. De Cecco⁷⁹, J. de Graat⁹⁹, N. De Groot¹⁰⁵,
 P. de Jong¹⁰⁶, C. De La Taille¹¹⁶, H. De la Torre⁸¹, F. De Lorenzi⁶³, L. De Nooij¹⁰⁶,
 D. De Pedis^{133a}, A. De Salvo^{133a}, U. De Sanctis^{165a,165c}, A. De Santo¹⁵⁰,
 J.B. De Vivie De Regie¹¹⁶, G. De Zorzi^{133a,133b}, W.J. Dearnaley⁷¹, R. Debbe²⁵,
 C. Debenedetti⁴⁶, B. Dechenaux⁵⁵, D.V. Dedovich⁶⁴, J. Degenhardt¹²¹, J. Del Peso⁸¹,
 T. Del Prete^{123a,123b}, T. Delemontex⁵⁵, M. Deliyergiyev⁷⁴, A. Dell'Acqua³⁰, L. Dell'Asta²²,
 M. Della Pietra^{103a,i}, D. della Volpe^{103a,103b}, M. Delmastro⁵, P.A. Delsart⁵⁵, C. Deluca¹⁰⁶,
 S. Demers¹⁷⁷, M. Demichev⁶⁴, A. Demilly⁷⁹, B. Demirkoz^{12,k}, S.P. Denisov¹²⁹,
 D. Derendarz³⁹, J.E. Derkaoui^{136d}, F. Derue⁷⁹, P. Dervan⁷³, K. Desch²¹, P.O. Deviveiros¹⁰⁶,

M. Limper⁶², S.C. Lin^{152,x}, F. Linde¹⁰⁶, B.E. Lindquist¹⁴⁹, J.T. Linnemann⁸⁹, E. Lipeles¹²¹,
A. Lipniacka¹⁴, M. Lisovsky⁴², T.M. Liss¹⁶⁶, D. Lissauer²⁵, A. Lister¹⁶⁹, A.M. Litke¹³⁸,
B. Liu¹⁵², D. Liu¹⁵², J.B. Liu^{33b}, K. Liu^{33b,y}, L. Liu⁸⁸, M. Liu⁴⁵, M. Liu^{33b}, Y. Liu^{33b},
M. Livan^{120a,120b}, S.S.A. Livermore¹¹⁹, A. Lleres⁵⁵, J. Llorente Merino⁸¹, S.L. Lloyd⁷⁵,
F. Lo Sterzo^{133a,133b}, E. Lobodzinska⁴², P. Loch⁷, W.S. Lockman¹³⁸, T. Loddenkoetter²¹,
F.K. Loebinger⁸³, A.E. Loevschall-Jensen³⁶, A. Loginov¹⁷⁷, C.W. Loh¹⁶⁹, T. Lohse¹⁶,
K. Lohwasser⁴⁸, M. Lokajicek¹²⁶, V.P. Lombardo⁵, R.E. Long⁷¹, L. Lopes^{125a},
D. Lopez Mateos⁵⁷, B. Lopez Paredes¹⁴⁰, J. Lorenz⁹⁹, N. Lorenzo Martinez¹¹⁶,
M. Losada¹⁶³, P. Loscutoff¹⁵, M.J. Losty^{160a,*}, X. Lou⁴¹, A. Lounis¹¹⁶, J. Love⁶, P.A. Love⁷¹,
A.J. Lowe^{144,f}, F. Lu^{33a}, H.J. Lubatti¹³⁹, C. Luci^{133a,133b}, A. Lucotte⁵⁵, D. Ludwig⁴²,
I. Ludwig⁴⁸, J. Ludwig⁴⁸, F. Luehring⁶⁰, W. Lukas⁶¹, L. Luminari^{133a}, E. Lund¹¹⁸,
J. Lundberg^{147a,147b}, O. Lundberg^{147a,147b}, B. Lund-Jensen¹⁴⁸, M. Lungwitz⁸², D. Lynn²⁵,
R. Lysak¹²⁶, E. Lytken⁸⁰, H. Ma²⁵, L.L. Ma^{33d}, G. Maccarrone⁴⁷, A. Macchiolo¹⁰⁰,
B. Mačec⁷⁴, J. Machado Miguens^{125a}, D. Macina³⁰, R. Mackeprang³⁶, R. Madar⁴⁸,
R.J. Madaras¹⁵, H.J. Maddocks⁷¹, W.F. Mader⁴⁴, A. Madsen¹⁶⁷, M. Maeno⁸, T. Maeno²⁵,
L. Magnoni¹⁶⁴, E. Magradze⁵⁴, K. Mahboubi⁴⁸, J. Mahlstedt¹⁰⁶, S. Mahmoud⁷³,
G. Mahout¹⁸, C. Maiani¹³⁷, C. Maidantchik^{24a}, A. Maio^{125a,c}, S. Majewski¹¹⁵, Y. Makida⁶⁵,
N. Makovec¹¹⁶, P. Mal^{137,z}, B. Malaescu⁷⁹, Pa. Malecki³⁹, V.P. Maleev¹²², F. Malek⁵⁵,
U. Mallik⁶², D. Malon⁶, C. Malone¹⁴⁴, S. Maltezos¹⁰, V.M. Malyshev¹⁰⁸, S. Malyukov³⁰,
J. Mamuzic^{13b}, L. Mandelli^{90a}, I. Mandić⁷⁴, R. Mandrysch⁶², J. Maneira^{125a},
A. Manfredini¹⁰⁰, L. Manhaes de Andrade Filho^{24b}, J.A. Manjarres Ramos¹³⁷, A. Mann⁹⁹,
P.M. Manning¹³⁸, A. Manousakis-Katsikakis⁹, B. Mansoulie¹³⁷, R. Mantifel⁸⁶, L. Mapelli³⁰,
L. March¹⁶⁸, J.F. Marchand²⁹, F. Marchese^{134a,134b}, G. Marchiori⁷⁹, M. Marcisovsky¹²⁶,
C.P. Marino¹⁷⁰, C.N. Marques^{125a}, F. Marroquim^{24a}, Z. Marshall¹⁵, L.F. Marti¹⁷,
S. Marti-Garcia¹⁶⁸, B. Martin³⁰, B. Martin⁸⁹, J.P. Martin⁹⁴, T.A. Martin¹⁷¹, V.J. Martin⁴⁶,
B. Martin dit Latour⁴⁹, H. Martinez¹³⁷, M. Martinez^{12,p}, S. Martin-Haugh¹⁵⁰,
A.C. Martyniuk¹⁷⁰, M. Marx⁸³, F. Marzano^{133a}, A. Marzin¹¹², L. Masetti⁸²,
T. Mashimo¹⁵⁶, R. Mashinistov⁹⁵, J. Masik⁸³, A.L. Maslennikov¹⁰⁸, I. Massa^{20a,20b},
N. Massol⁵, P. Mastrandrea¹⁴⁹, A. Mastroberardino^{37a,37b}, T. Masubuchi¹⁵⁶,
H. Matsunaga¹⁵⁶, T. Matsushita⁶⁶, P. Mättig¹⁷⁶, S. Mättig⁴², J. Mattmann⁸²,
C. Matting^{119,d}, J. Maurer⁸⁴, S.J. Maxfield⁷³, D.A. Maximov^{108,g}, R. Mazini¹⁵²,
L. Mazzaferro^{134a,134b}, M. Mazzanti^{90a}, S.P. Mc Kee⁸⁸, A. McCarn¹⁶⁶, R.L. McCarthy¹⁴⁹,
T.G. McCarthy²⁹, N.A. McCubbin¹³⁰, K.W. McFarlane^{56,*}, J.A. McFayden¹⁴⁰,
G. Mchedlidze^{51b}, T. McLaughlan¹⁸, S.J. McMahon¹³⁰, R.A. McPherson^{170,j}, A. Meade⁸⁵,
J. Mechnich¹⁰⁶, M. Mechtel¹⁷⁶, M. Medinnis⁴², S. Meehan³¹, R. Meera-Lebbai¹¹²,
S. Mehlhase³⁶, A. Mehta⁷³, K. Meier^{58a}, C. Meineck⁹⁹, B. Meirose⁸⁰, C. Melachrinou³¹,
B.R. Mellado Garcia^{146c}, F. Meloni^{90a,90b}, L. Mendoza Navas¹⁶³, A. Mengarelli^{20a,20b},
S. Menke¹⁰⁰, E. Meoni¹⁶², K.M. Mercurio⁵⁷, S. Mergelmeyer²¹, N. Meric¹³⁷, P. Mermod⁴⁹,
L. Merola^{103a,103b}, C. Meroni^{90a}, F.S. Merritt³¹, H. Merritt¹¹⁰, A. Messina^{30,aa},
J. Metcalfe²⁵, A.S. Mete¹⁶⁴, C. Meyer⁸², C. Meyer³¹, J-P. Meyer¹³⁷, J. Meyer³⁰, J. Meyer⁵⁴,
S. Michal³⁰, R.P. Middleton¹³⁰, S. Migas⁷³, L. Mijović¹³⁷, G. Mikenberg¹⁷³,
M. Míkestikova¹²⁶, M. Mikuž⁷⁴, D.W. Miller³¹, W.J. Mills¹⁶⁹, C. Mills⁵⁷, A. Milov¹⁷³,
D.A. Milstead^{147a,147b}, D. Milstein¹⁷³, A.A. Minaenko¹²⁹, M. Miñano Moya¹⁶⁸,
I.A. Minashvili⁶⁴, A.I. Mincer¹⁰⁹, B. Mindur^{38a}, M. Mineev⁶⁴, Y. Ming¹⁷⁴, L.M. Mir¹²,
G. Mirabelli^{133a}, T. Mitani¹⁷², J. Mitrevski¹³⁸, V.A. Mitsou¹⁶⁸, S. Mitsui⁶⁵,
P.S. Miyagawa¹⁴⁰, J.U. Mjörnmark⁸⁰, T. Moa^{147a,147b}, V. Moeller²⁸, S. Mohapatra¹⁴⁹,
W. Mohr⁴⁸, S. Molander^{147a,147b}, R. Moles-Valls¹⁶⁸, A. Molfetas³⁰, K. Mönig⁴²,
C. Monini⁵⁵, J. Monk³⁶, E. Monnier⁸⁴, J. Montejo Berlingen¹², F. Monticelli⁷⁰,
S. Monzani^{20a,20b}, R.W. Moore³, C. Mora Herrera⁴⁹, A. Moraes⁵³, N. Morange⁶²,
J. Morel⁵⁴, D. Moreno⁸², M. Moreno Llácer¹⁶⁸, P. Morettini^{50a}, M. Morgenstern⁴⁴,
M. Morii⁵⁷, S. Moritz⁸², A.K. Morley¹⁴⁸, G. Mornacchi³⁰, J.D. Morris⁷⁵, L. Morvaj¹⁰²,
H.G. Moser¹⁰⁰, M. Mosidze^{51b}, J. Moss¹¹⁰, R. Mount¹⁴⁴, E. Mountricha^{10,ab},

S.V. Mouraviev^{95,*}, E.J.W. Moyse⁸⁵, R.D. Mudd¹⁸, F. Mueller^{58a}, J. Mueller¹²⁴, K. Mueller²¹, T. Mueller²⁸, T. Mueller⁸², D. Muenstermann⁴⁹, Y. Munwes¹⁵⁴, J.A. Murillo Quijada¹⁸, W.J. Murray¹³⁰, I. Mussche¹⁰⁶, E. Musto¹⁵³, A.G. Myagkov^{129,ac}, M. Myska¹²⁶, O. Nackenhorst⁵⁴, J. Nadal¹², K. Nagai⁶¹, R. Nagai¹⁵⁸, Y. Nagai⁸⁴, K. Nagano⁶⁵, A. Nagarkar¹¹⁰, Y. Nagasaka⁵⁹, M. Nagel¹⁰⁰, A.M. Nairz³⁰, Y. Nakahama³⁰, K. Nakamura⁶⁵, T. Nakamura¹⁵⁶, I. Nakano¹¹¹, H. Namasivayam⁴¹, G. Nanava²¹, A. Napier¹⁶², R. Narayan^{58b}, M. Nash^{77,d}, T. Nattermann²¹, T. Naumann⁴², G. Navarro¹⁶³, H.A. Neal⁸⁸, P.Yu. Nechaeva⁹⁵, T.J. Neep⁸³, A. Negri^{120a,120b}, G. Negri³⁰, M. Negrini^{20a}, S. Nektarijevic⁴⁹, A. Nelson¹⁶⁴, T.K. Nelson¹⁴⁴, S. Nemecek¹²⁶, P. Nemethy¹⁰⁹, A.A. Nepomuceno^{24a}, M. Nessi^{30,ad}, M.S. Neubauer¹⁶⁶, M. Neumann¹⁷⁶, A. Neusiedl⁸², R.M. Neves¹⁰⁹, P. Nevski²⁵, F.M. Newcomer¹²¹, P.R. Newman¹⁸, D.H. Nguyen⁶, V. Nguyen Thi Hong¹³⁷, R.B. Nickerson¹¹⁹, R. Nicolaidou¹³⁷, B. Nicquevert³⁰, J. Nielsen¹³⁸, N. Nikiforou³⁵, A. Nikiforov¹⁶, V. Nikolaenko^{129,ac}, I. Nikolic-Audit⁷⁹, K. Nikolics⁴⁹, K. Nikolopoulos¹⁸, P. Nilsson⁸, Y. Ninomiya¹⁵⁶, A. Nisati^{133a}, R. Nisius¹⁰⁰, T. Nobe¹⁵⁸, L. Nodulman⁶, M. Nomachi¹¹⁷, I. Nomidis¹⁵⁵, S. Norberg¹¹², M. Nordberg³⁰, J. Novakova¹²⁸, M. Nozaki⁶⁵, L. Nozka¹¹⁴, K. Ntekas¹⁰, A.-E. Nuncio-Quiroz²¹, G. Nunes Hanninger⁸⁷, T. Nunnemann⁹⁹, E. Nurse⁷⁷, B.J. O'Brien⁴⁶, F. O'grady⁷, D.C. O'Neil¹⁴³, V. O'Shea⁵³, L.B. Oakes⁹⁹, F.G. Oakham^{29,e}, H. Oberlack¹⁰⁰, J. Ocariz⁷⁹, A. Ochi⁶⁶, M.I. Ochoa⁷⁷, S. Oda⁶⁹, S. Odaka⁶⁵, J. Odier⁸⁴, H. Ogren⁶⁰, A. Oh⁸³, S.H. Oh⁴⁵, C.C. Ohm³⁰, T. Ohshima¹⁰², W. Okamura¹¹⁷, H. Okawa²⁵, Y. Okumura³¹, T. Okuyama¹⁵⁶, A. Olariu^{26a}, A.G. Olchevski⁶⁴, S.A. Olivares Pino⁴⁶, M. Oliveira^{125a,h}, D. Oliveira Damazio²⁵, E. Oliver Garcia¹⁶⁸, D. Olivito¹²¹, A. Olszewski³⁹, J. Olszowska³⁹, A. Onofre^{125a,ae}, P.U.E. Onyisi^{31,af}, C.J. Oram^{160a}, M.J. Oreglia³¹, Y. Oren¹⁵⁴, D. Orestano^{135a,135b}, N. Orlando^{72a,72b}, C. Oropeza Barrera⁵³, R.S. Orr¹⁵⁹, B. Osculati^{50a,50b}, R. Ospanov¹²¹, G. Otero y Garzon²⁷, H. Otono⁶⁹, J.P. Ottersbach¹⁰⁶, M. Ouchrif^{136d}, E.A. Ouellette¹⁷⁰, F. Ould-Saada¹¹⁸, A. Ouraou¹³⁷, K.P. Oussoren¹⁰⁶, Q. Ouyang^{33a}, A. Ovcharova¹⁵, M. Owen⁸³, S. Owen¹⁴⁰, V.E. Ozcan^{19a}, N. Ozturk⁸, K. Pachal¹¹⁹, A. Pacheco Pages¹², C. Padilla Aranda¹², S. Pagan Griso¹⁵, E. Paganis¹⁴⁰, C. Pahl¹⁰⁰, F. Paige²⁵, P. Pais⁸⁵, K. Pajchel¹¹⁸, G. Palacino^{160b}, C.P. Paleari⁷, S. Palestini³⁰, D. Pallin³⁴, A. Palma^{125a}, J.D. Palmer¹⁸, Y.B. Pan¹⁷⁴, E. Panagiotopoulou¹⁰, J.G. Panduro Vazquez⁷⁶, P. Pani¹⁰⁶, N. Panikashvili⁸⁸, S. Panitkin²⁵, D. Pantea^{26a}, A. Papadellis^{147a}, Th.D. Papadopoulou¹⁰, K. Papageorgiou^{155,o}, A. Paramonov⁶, D. Paredes Hernandez³⁴, M.A. Parker²⁸, F. Parodi^{50a,50b}, J.A. Parsons³⁵, U. Parzefall⁴⁸, S. Pashapour⁵⁴, E. Pasqualucci^{133a}, S. Passaggio^{50a}, A. Passeri^{135a}, F. Pastore^{135a,135b,*}, Fr. Pastore⁷⁶, G. Pásztor^{49,ag}, S. Pataraiia¹⁷⁶, N.D. Patel¹⁵¹, J.R. Pater⁸³, S. Patricelli^{103a,103b}, T. Pauly³⁰, J. Pearce¹⁷⁰, M. Pedersen¹¹⁸, S. Pedraza Lopez¹⁶⁸, M.I. Pedraza Morales¹⁷⁴, S.V. Peleganchuk¹⁰⁸, D. Pelikan¹⁶⁷, H. Peng^{33b}, B. Penning³¹, A. Penson³⁵, J. Penwell⁶⁰, D.V. Perepelitsa³⁵, T. Perez Cavalcanti⁴², E. Perez Codina^{160a}, M.T. Pérez García-Estañ¹⁶⁸, V. Perez Reale³⁵, L. Perini^{90a,90b}, H. Pernegger³⁰, R. Perrino^{72a}, V.D. Peshekhonov⁶⁴, K. Peters³⁰, R.F.Y. Peters^{54,ah}, B.A. Petersen³⁰, J. Petersen³⁰, T.C. Petersen³⁶, E. Petit⁵, A. Petridis^{147a,147b}, C. Petridou¹⁵⁵, E. Petrolo^{133a}, F. Petrucci^{135a,135b}, M. Petteni¹⁴³, R. Pezoa^{32b}, P.W. Phillips¹³⁰, G. Piacquadio¹⁴⁴, E. Pianori¹⁷¹, A. Picazio⁴⁹, E. Piccaro⁷⁵, M. Piccinini^{20a,20b}, S.M. Piec⁴², R. Piegai²⁷, D.T. Pignotti¹¹⁰, J.E. Pilcher³¹, A.D. Pilkington⁷⁷, J. Pina^{125a,c}, M. Pinamonti^{165a,165c,ai}, A. Pinder¹¹⁹, J.L. Pinfold³, A. Pingel³⁶, B. Pinto^{125a}, C. Pizio^{90a,90b}, M.-A. Pleier²⁵, V. Pleskot¹²⁸, E. Plotnikova⁶⁴, P. Plucinski^{147a,147b}, S. Poddar^{58a}, F. Podlyski³⁴, R. Poettgen⁸², L. Poggioli¹¹⁶, D. Pohl²¹, M. Pohl⁴⁹, G. Polesello^{120a}, A. Policicchio^{37a,37b}, R. Polifka¹⁵⁹, A. Polini^{20a}, C.S. Pollard⁴⁵, V. Polychronakos²⁵, D. Pomeroy²³, K. Pommès³⁰, L. Pontecorvo^{133a}, B.G. Pope⁸⁹, G.A. Popeneciu^{26b}, D.S. Popovic^{13a}, A. Poppleton³⁰, X. Portell Bueso¹², G.E. Pospelov¹⁰⁰, S. Pospisil¹²⁷, I.N. Potrap⁶⁴, C.J. Potter¹⁵⁰, C.T. Potter¹¹⁵, G. Poulard³⁰, J. Poveda⁶⁰, V. Pozdnyakov⁶⁴, R. Prabhu⁷⁷, P. Pralavorio⁸⁴, A. Pranko¹⁵, S. Prasad³⁰, R. Pravahan²⁵, S. Prell⁶³, D. Price⁶⁰, J. Price⁷³,

L.E. Price⁶, D. Prieur¹²⁴, M. Primavera^{72a}, M. Proissl⁴⁶, K. Prokofiev¹⁰⁹, F. Prokoshin^{32b}, E. Protopapadaki¹³⁷, S. Protopopescu²⁵, J. Proudfoot⁶, X. Prudent⁴⁴, M. Przybycien^{38a}, H. Przysiezniak⁵, S. Psoroulas²¹, E. Ptacek¹¹⁵, E. Pueschel⁸⁵, D. Puldon¹⁴⁹, M. Purohit^{25,aj}, P. Puzo¹¹⁶, Y. Pylypchenko⁶², J. Qian⁸⁸, A. Quadt⁵⁴, D.R. Quarrie¹⁵, W.B. Quayle^{146c}, D. Quilty⁵³, V. Radeka²⁵, V. Radescu⁴², P. Radloff¹¹⁵, F. Ragusa^{90a,90b}, G. Rahal¹⁷⁹, S. Rajagopalan²⁵, M. Rammensee⁴⁸, M. Rammes¹⁴², A.S. Randle-Conde⁴⁰, C. Rangel-Smith⁷⁹, K. Rao¹⁶⁴, F. Rauscher⁹⁹, T.C. Rave⁴⁸, T. Ravenscroft⁵³, M. Raymond³⁰, A.L. Read¹¹⁸, D.M. Rebuffi^{120a,120b}, A. Redelbach¹⁷⁵, G. Redlinger²⁵, R. Reece¹²¹, K. Reeves⁴¹, A. Reinsch¹¹⁵, I. Reisinger⁴³, M. Relich¹⁶⁴, C. Rembser³⁰, Z.L. Ren¹⁵², A. Renaud¹¹⁶, M. Rescigno^{133a}, S. Resconi^{90a}, B. Resende¹³⁷, P. Reznicek⁹⁹, R. Rezvani⁹⁴, R. Richter¹⁰⁰, E. Richter-Was^{38b}, M. Ridel⁷⁹, P. Rieck¹⁶, M. Rijssenbeek¹⁴⁹, A. Rimoldi^{120a,120b}, L. Rinaldi^{20a}, R.R. Rios⁴⁰, E. Ritsch⁶¹, I. Riu¹², G. Rivoltella^{90a,90b}, F. Rizatdinova¹¹³, E. Rizvi⁷⁵, S.H. Robertson^{86,j}, A. Robichaud-Veronneau¹¹⁹, D. Robinson²⁸, J.E.M. Robinson⁸³, A. Robson⁵³, J.G. Rocha de Lima¹⁰⁷, C. Roda^{123a,123b}, D. Roda Dos Santos¹²⁶, L. Rodrigues³⁰, A. Roe⁵⁴, S. Roe³⁰, O. Röhne¹¹⁸, S. Rolli¹⁶², A. Romaniouk⁹⁷, M. Romano^{20a,20b}, G. Romeo²⁷, E. Romero Adam¹⁶⁸, N. Rompotis¹³⁹, L. Roos⁷⁹, E. Ros¹⁶⁸, S. Rosati^{133a}, K. Rosbach⁴⁹, A. Rose¹⁵⁰, M. Rose⁷⁶, P.L. Rosendahl¹⁴, O. Rosenthal¹⁴², V. Rossetti¹², E. Rossi^{133a,133b}, L.P. Rossi^{50a}, R. Rosten¹³⁹, M. Rotaru^{26a}, I. Roth¹⁷³, J. Rothberg¹³⁹, D. Rousseau¹¹⁶, C.R. Royon¹³⁷, A. Rozanov⁸⁴, Y. Rozen¹⁵³, X. Ruan^{146c}, F. Rubbo¹², I. Rubinskiy⁴², N. Ruckstuhl¹⁰⁶, V.I. Rud⁹⁸, C. Rudolph⁴⁴, M.S. Rudolph¹⁵⁹, F. Rühr⁷, A. Ruiz-Martinez⁶³, L. Rumyantsev⁶⁴, Z. Rurikova⁴⁸, N.A. Rusakovich⁶⁴, A. Ruschke⁹⁹, J.P. Rutherford⁷, N. Ruthmann⁴⁸, P. Ruzicka¹²⁶, Y.F. Ryabov¹²², M. Rybar¹²⁸, G. Rybkin¹¹⁶, N.C. Ryder¹¹⁹, A.F. Saavedra¹⁵¹, A. Saddique³, I. Sadeh¹⁵⁴, H.F.W. Sadrozinski¹³⁸, R. Sadykov⁶⁴, F. Safai Tehrani^{133a}, H. Sakamoto¹⁵⁶, G. Salamanna⁷⁵, A. Salamon^{134a}, M. Saleem¹¹², D. Salek³⁰, D. Salihagic¹⁰⁰, A. Salnikov¹⁴⁴, J. Salt¹⁶⁸, B.M. Salvachua Ferrando⁶, D. Salvatore^{37a,37b}, F. Salvatore¹⁵⁰, A. Salvucci¹⁰⁵, A. Salzburger³⁰, D. Sampsonidis¹⁵⁵, A. Sanchez^{103a,103b}, J. Sánchez¹⁶⁸, V. Sanchez Martinez¹⁶⁸, H. Sandaker¹⁴, H.G. Sander⁸², M.P. Sanders⁹⁹, M. Sandhoff¹⁷⁶, T. Sandoval²⁸, C. Sandoval¹⁶³, R. Sandstroem¹⁰⁰, D.P.C. Sankey¹³⁰, A. Sansoni⁴⁷, C. Santoni³⁴, R. Santonico^{134a,134b}, H. Santos^{125a}, I. Santoyo Castillo¹⁵⁰, K. Sapp¹²⁴, A. Sapronov⁶⁴, J.G. Saraiva^{125a}, T. Sarangi¹⁷⁴, E. Sarkisyan-Grinbaum⁸, B. Sarrazin²¹, F. Sarri^{123a,123b}, G. Sartisohn¹⁷⁶, O. Sasaki⁶⁵, Y. Sasaki¹⁵⁶, N. Sasao⁶⁷, I. Satsounkevitch⁹¹, G. Sauvage^{5,*}, E. Sauvan⁵, J.B. Sauvan¹¹⁶, P. Savard^{159,e}, V. Savinov¹²⁴, D.O. Savu³⁰, C. Sawyer¹¹⁹, L. Sawyer^{78,l}, D.H. Saxon⁵³, J. Saxon¹²¹, C. Sbarra^{20a}, A. Sbrizzi³, T. Scanlon³⁰, D.A. Scannicchio¹⁶⁴, M. Scarcella¹⁵¹, J. Schaarschmidt¹¹⁶, P. Schacht¹⁰⁰, D. Schaefer¹²¹, A. Schaelicke⁴⁶, S. Schaepe²¹, S. Schaetzel^{58b}, U. Schäfer⁸², A.C. Schaffer¹¹⁶, D. Schaile⁹⁹, R.D. Schamberger¹⁴⁹, V. Scharf^{58a}, V.A. Schegelsky¹²², D. Scheirich⁸⁸, M. Schernau¹⁶⁴, M.I. Scherzer³⁵, C. Schiavi^{50a,50b}, J. Schieck⁹⁹, C. Schillo⁴⁸, M. Schioppa^{37a,37b}, S. Schlenker³⁰, E. Schmidt⁴⁸, K. Schmieden²¹, C. Schmitt⁸², C. Schmitt⁹⁹, S. Schmitt^{58b}, B. Schneider¹⁷, Y.J. Schnellbach⁷³, U. Schnoor⁴⁴, L. Schoeffel¹³⁷, A. Schoening^{58b}, A.L.S. Schorlemmer⁵⁴, M. Schott⁸², D. Schouten^{160a}, J. Schovancova¹²⁶, M. Schram⁸⁶, C. Schroeder⁸², N. Schroer^{58c}, N. Schuh⁸², M.J. Schultens²¹, H.-C. Schultz-Coulon^{58a}, H. Schulz¹⁶, M. Schumacher⁴⁸, B.A. Schumm¹³⁸, Ph. Schune¹³⁷, A. Schwartzman¹⁴⁴, Ph. Schwegler¹⁰⁰, Ph. Schwemling¹³⁷, R. Schwienhorst⁸⁹, J. Schwindling¹³⁷, T. Schwindt²¹, M. Schwoerer⁵, F.G. Sciacca¹⁷, E. Scifo¹¹⁶, G. Sciolla²³, W.G. Scott¹³⁰, F. Scutti²¹, J. Searcy⁸⁸, G. Sedov⁴², E. Sedykh¹²², S.C. Seidel¹⁰⁴, A. Seiden¹³⁸, F. Seifert⁴⁴, J.M. Seixas^{24a}, G. Sekhniaidze^{103a}, S.J. Sekula⁴⁰, K.E. Selbach⁴⁶, D.M. Seliverstov¹²², G. Sellers⁷³, M. Seman^{145b}, N. Semprini-Cesari^{20a,20b}, C. Serfon³⁰, L. Serin¹¹⁶, L. Serkin⁵⁴, T. Serre⁸⁴, R. Seuster^{160a}, H. Severini¹¹², F. Sforza¹⁰⁰, A. Sfyrla³⁰, E. Shabalina⁵⁴, M. Shamim¹¹⁵, L.Y. Shan^{33a}, J.T. Shank²², Q.T. Shao⁸⁷, M. Shapiro¹⁵, P.B. Shatalov⁹⁶, K. Shaw^{165a,165c}, P. Sherwood⁷⁷, S. Shimizu⁶⁶, M. Shimojima¹⁰¹, T. Shin⁵⁶, M. Shiyakova⁶⁴, A. Shmeleva⁹⁵, M.J. Shochet³¹,

D. Short¹¹⁹, S. Shrestha⁶³, E. Shulga⁹⁷, M.A. Shupe⁷, S. Shushkevich⁴², P. Sicho¹²⁶,
 D. Sidorov¹¹³, A. Sidoti^{133a}, F. Siegert⁴⁸, Dj. Sijacki^{13a}, O. Silbert¹⁷³, J. Silva^{125a},
 Y. Silver¹⁵⁴, D. Silverstein¹⁴⁴, S.B. Silverstein^{147a}, V. Simak¹²⁷, O. Simard⁵, Lj. Simic^{13a},
 S. Simion¹¹⁶, E. Simioni⁸², B. Simmons⁷⁷, R. Simoniello^{90a,90b}, M. Simonyan³⁶,
 P. Sinervo¹⁵⁹, N.B. Sinev¹¹⁵, V. Sipica¹⁴², G. Siragusa¹⁷⁵, A. Sircar⁷⁸, A.N. Sisakyan^{64,*},
 S.Yu. Sivoklov⁹⁸, J. Sjölin^{147a,147b}, T.B. Sjursen¹⁴, L.A. Skinnari¹⁵, H.P. Skottowe⁵⁷,
 K.Yu. Skovpen¹⁰⁸, P. Skubic¹¹², M. Slater¹⁸, T. Slavicek¹²⁷, K. Sliwa¹⁶², V. Smakhtin¹⁷³,
 B.H. Smart⁴⁶, L. Smestad¹¹⁸, S.Yu. Smirnov⁹⁷, Y. Smirnov⁹⁷, L.N. Smirnova^{98.ak},
 O. Smirnova⁸⁰, K.M. Smith⁵³, M. Smizanska⁷¹, K. Smolek¹²⁷, A.A. Snesarev⁹⁵,
 G. Snidero⁷⁵, J. Snow¹¹², S. Snyder²⁵, R. Sobie^{170.j}, J. Sodomka¹²⁷, A. Soffer¹⁵⁴,
 D.A. Soh^{152.w}, C.A. Solans³⁰, M. Solar¹²⁷, J. Solc¹²⁷, E.Yu. Soldatov⁹⁷, U. Soldevila¹⁶⁸,
 E. Solfaroli Camillocci^{133a,133b}, A.A. Solodkov¹²⁹, O.V. Solovyanov¹²⁹, V. Solovyev¹²²,
 N. Soni¹, A. Sood¹⁵, V. Sopko¹²⁷, B. Sopko¹²⁷, M. Sosebee⁸, R. Soualah^{165a,165c},
 P. Soueid⁹⁴, A.M. Soukharev¹⁰⁸, D. South⁴², S. Spagnolo^{72a,72b}, F. Spanò⁷⁶,
 W.R. Spearman⁵⁷, R. Spighi^{20a}, G. Spigo³⁰, M. Spousta^{128.al}, T. Spreitzer¹⁵⁹, B. Spurlock⁸,
 R.D. St. Denis⁵³, J. Stahlman¹²¹, R. Stamen^{58a}, E. Stanecka³⁹, R.W. Stanek⁶,
 C. Stanescu^{135a}, M. Stanescu-Bellu⁴², M.M. Stanitzki⁴², S. Stapnes¹¹⁸, E.A. Starchenko¹²⁹,
 J. Stark⁵⁵, P. Staroba¹²⁶, P. Starovoitov⁴², R. Staszewski³⁹, A. Staude⁹⁹, P. Stavina^{145a,*},
 G. Steele⁵³, P. Steinbach⁴⁴, P. Steinberg²⁵, I. Stekl¹²⁷, B. Stelzer¹⁴³, H.J. Stelzer⁸⁹,
 O. Stelzer-Chilton^{160a}, H. Stenzel⁵², S. Stern¹⁰⁰, G.A. Stewart³⁰, J.A. Stillings²¹,
 M.C. Stockton⁸⁶, M. Stoebe⁸⁶, K. Stoerig⁴⁸, G. Stoicea^{26a}, S. Stonjek¹⁰⁰, A.R. Stradling⁸,
 A. Straessner⁴⁴, J. Strandberg¹⁴⁸, S. Strandberg^{147a,147b}, A. Strandlie¹¹⁸, E. Strauss¹⁴⁴,
 M. Strauss¹¹², P. Strizenc^{145b}, R. Ströhmer¹⁷⁵, D.M. Strom¹¹⁵, R. Stroynowski⁴⁰,
 B. Stugu¹⁴, I. Stumer^{25.*}, J. Stupak¹⁴⁹, P. Sturm¹⁷⁶, N.A. Styles⁴², D. Su¹⁴⁴,
 HS. Subramania³, R. Subramaniam⁷⁸, A. Succurro¹², Y. Sugaya¹¹⁷, C. Suhr¹⁰⁷, M. Suk¹²⁷,
 V.V. Sulini⁹⁵, S. Sultansoy^{4c}, T. Sumida⁶⁷, X. Sun⁵⁵, J.E. Sundermann⁴⁸, K. Suruliz¹⁴⁰,
 G. Susinno^{37a,37b}, M.R. Sutton¹⁵⁰, Y. Suzuki⁶⁵, M. Svatos¹²⁶, S. Swedish¹⁶⁹,
 M. Swiatlowski¹⁴⁴, I. Sykora^{145a}, T. Sykora¹²⁸, D. Ta¹⁰⁶, K. Tackmann⁴², A. Taffard¹⁶⁴,
 R. Tahirout^{160a}, N. Taiblum¹⁵⁴, Y. Takahashi¹⁰², H. Takai²⁵, R. Takashima⁶⁸, H. Takeda⁶⁶,
 T. Takeshita¹⁴¹, Y. Takubo⁶⁵, M. Talby⁸⁴, A.A. Talyshv^{108.g}, J.Y.C. Tam¹⁷⁵,
 M.C. Tamsett^{78.am}, K.G. Tan⁸⁷, J. Tanaka¹⁵⁶, R. Tanaka¹¹⁶, S. Tanaka¹³², S. Tanaka⁶⁵,
 A.J. Tanasijczuk¹⁴³, K. Tani⁶⁶, N. Tannoury⁸⁴, S. Tapprogge⁸², S. Tarem¹⁵³, F. Tarrade²⁹,
 G.F. Tartarelli^{90a}, P. Tas¹²⁸, M. Tasevsky¹²⁶, T. Tashiro⁶⁷, E. Tassi^{37a,37b},
 A. Tavares Delgado^{125a}, Y. Tayalati^{136d}, C. Taylor⁷⁷, F.E. Taylor⁹³, G.N. Taylor⁸⁷,
 W. Taylor^{160b}, M. Teinturier¹¹⁶, F.A. Teischinger³⁰, M. Teixeira Dias Castanheira⁷⁵,
 P. Teixeira-Dias⁷⁶, K.K. Temming⁴⁸, H. Ten Kate³⁰, P.K. Teng¹⁵², S. Terada⁶⁵, K. Terashi¹⁵⁶,
 J. Terron⁸¹, M. Testa⁴⁷, R.J. Teuscher^{159.j}, J. Therhaag²¹, T. Theveneaux-Pelzer³⁴,
 S. Thoma⁴⁸, J.P. Thomas¹⁸, E.N. Thompson³⁵, P.D. Thompson¹⁸, P.D. Thompson¹⁵⁹,
 A.S. Thompson⁵³, L.A. Thomsen³⁶, E. Thomson¹²¹, M. Thomson²⁸, W.M. Thong⁸⁷,
 R.P. Thun^{88.*}, F. Tian³⁵, M.J. Tibbetts¹⁵, T. Tic¹²⁶, V.O. Tikhomirov⁹⁵, Yu.A. Tikhonov^{108.g},
 S. Timoshenko⁹⁷, E. Tiouchichine⁸⁴, P. Tipton¹⁷⁷, S. Tisserant⁸⁴, T. Todorov⁵,
 S. Todorova-Nova¹²⁸, B. Toggerson¹⁶⁴, J. Tojo⁶⁹, S. Tokár^{145a}, K. Tokushuku⁶⁵,
 K. Tollefson⁸⁹, L. Tomlinson⁸³, M. Tomoto¹⁰², L. Tompkins³¹, K. Toms¹⁰⁴, A. Tonoyan¹⁴,
 C. Topfel¹⁷, N.D. Topilin⁶⁴, E. Torrence¹¹⁵, H. Torres⁷⁹, E. Torrò Pastor¹⁶⁸, J. Toth^{84.ag},
 F. Touchard⁸⁴, D.R. Tovey¹⁴⁰, H.L. Tran¹¹⁶, T. Trefzger¹⁷⁵, L. Tremblet³⁰, A. Tricoli³⁰,
 I.M. Trigger^{160a}, S. Trincaz-Duvoid⁷⁹, M.F. Tripiama⁷⁰, N. Triplett²⁵, W. Trischuk¹⁵⁹,
 B. Trocmé⁵⁵, C. Troncon^{90a}, M. Trotter-McDonald¹⁴³, M. Trovatielli^{135a,135b}, P. True⁸⁹,
 M. Trzebinski³⁹, A. Trzupek³⁹, C. Tsarouchas³⁰, J.C.-L. Tseng¹¹⁹, P.V. Tsiarehka⁹¹,
 D. Tsionou¹³⁷, G. Tsipolitis¹⁰, S. Tsiskaridze¹², V. Tsiskaridze⁴⁸, E.G. Tskhadadze^{51a},
 I.I. Tsukerman⁹⁶, V. Tsulaia¹⁵, J.-W. Tsung²¹, S. Tsuno⁶⁵, D. Tsybychev¹⁴⁹, A. Tua¹⁴⁰,
 A. Tudorache^{26a}, V. Tudorache^{26a}, J.M. Tuggle³¹, A.N. Tuna¹²¹, S. Turchikhin^{98.ak},
 D. Turecek¹²⁷, I. Turk Cakir^{4d}, R. Turra^{90a,90b}, P.M. Tuts³⁵, A. Tykhonov⁷⁴,

M. Tylmad^{147a,147b}, M. Tyndel¹³⁰, K. Uchida²¹, I. Ueda¹⁵⁶, R. Ueno²⁹, M. Ughetto⁸⁴, M. Uglanđ¹⁴, M. Uhlenbrock²¹, F. Ukegawa¹⁶¹, G. Unal³⁰, A. Undrus²⁵, G. Unel¹⁶⁴, F.C. Ungaro⁴⁸, Y. Unno⁶⁵, D. Urbaniec³⁵, P. Urquijo²¹, G. Usai⁸, A. Usanova⁶¹, L. Vacavant⁸⁴, V. Vacek¹²⁷, B. Vachon⁸⁶, S. Vahsen¹⁵, N. Valencic¹⁰⁶, S. Valentinetti^{20a,20b}, A. Valero¹⁶⁸, L. Valery³⁴, S. Valkar¹²⁸, E. Valladolid Gallego¹⁶⁸, S. Vallecorosa⁴⁹, J.A. Valls Ferrer¹⁶⁸, R. Van Berg¹²¹, P.C. Van Der Deijl¹⁰⁶, R. van der Geer¹⁰⁶, H. van der Graaf¹⁰⁶, R. Van Der Leeuw¹⁰⁶, D. van der Ster³⁰, N. van Eldik³⁰, P. van Gemmeren⁶, J. Van Nieuwkoop¹⁴³, I. van Vulpen¹⁰⁶, M. Vanadia¹⁰⁰, W. Vandelli³⁰, A. Vaniachine⁶, P. Vankov⁴², F. Vannucci⁷⁹, R. Vari^{133a}, E.W. Varnes⁷, T. Varol⁸⁵, D. Varouchas¹⁵, A. Vartapetian⁸, K.E. Varvell¹⁵¹, V.I. Vassilakopoulos⁵⁶, F. Vazeille³⁴, T. Vazquez Schroeder⁵⁴, J. Veatch⁷, F. Veloso^{125a}, S. Veneziano^{133a}, A. Ventura^{72a,72b}, D. Ventura⁸⁵, M. Venturi⁴⁸, N. Venturi¹⁵⁹, V. Vercesi^{120a}, M. Verducci¹³⁹, W. Verkerke¹⁰⁶, J.C. Vermeulen¹⁰⁶, A. Vest⁴⁴, M.C. Vetterli^{143,e}, I. Vichou¹⁶⁶, T. Vickey^{146c,an}, O.E. Vickey Boeriu^{146c}, G.H.A. Viehhauser¹¹⁹, S. Viel¹⁶⁹, R. Vigne³⁰, M. Villa^{20a,20b}, M. Villaplana Perez¹⁶⁸, E. Vilucchi⁴⁷, M.G. Vincker²⁹, V.B. Vinogradov⁶⁴, J. Virzi¹⁵, O. Vitells¹⁷³, M. Viti⁴², I. Vivarelli⁴⁸, F. Vives Vaque³, S. Vlachos¹⁰, D. Vladoiu⁹⁹, M. Vlasak¹²⁷, A. Vogel²¹, P. Vokac¹²⁷, G. Volpi⁴⁷, M. Volpi⁸⁷, G. Volpini^{90a}, H. von der Schmitt¹⁰⁰, H. von Radziewski⁴⁸, E. von Toerne²¹, V. Vorobel¹²⁸, M. Vos¹⁶⁸, R. Voss³⁰, J.H. Vosseveld⁷³, N. Vranjes¹³⁷, M. Vranjes Milosavljevic¹⁰⁶, V. Vrba¹²⁶, M. Vreeswijk¹⁰⁶, T. Vu Anh⁴⁸, R. Vuillermet³⁰, I. Vukotic³¹, Z. Vykydal¹²⁷, W. Wagner¹⁷⁶, P. Wagner²¹, S. Wahrmond⁴⁴, J. Wakabayashi¹⁰², S. Walch⁸⁸, J. Walder⁷¹, R. Walker⁹⁹, W. Walkowiak¹⁴², R. Wall¹⁷⁷, P. Waller⁷³, B. Walsh¹⁷⁷, C. Wang⁴⁵, H. Wang¹⁷⁴, H. Wang⁴⁰, J. Wang¹⁵², J. Wang^{33a}, K. Wang⁸⁶, R. Wang¹⁰⁴, S.M. Wang¹⁵², T. Wang²¹, X. Wang¹⁷⁷, A. Warburton⁸⁶, C.P. Ward²⁸, D.R. Wardrope⁷⁷, M. Warsinsky⁴⁸, A. Washbrook⁴⁶, C. Wasicki⁴², I. Watanabe⁶⁶, P.M. Watkins¹⁸, A.T. Watson¹⁸, I.J. Watson¹⁵¹, M.F. Watson¹⁸, G. Watts¹³⁹, S. Watts⁸³, A.T. Waugh¹⁵¹, B.M. Waugh⁷⁷, S. Webb⁸³, M.S. Weber¹⁷, J.S. Webster³¹, A.R. Weidberg¹¹⁹, P. Weigell¹⁰⁰, J. Weingarten⁵⁴, C. Weiser⁴⁸, H. Weits¹⁰⁶, P.S. Wells³⁰, T. Wenaus²⁵, D. Wendland¹⁶, Z. Weng^{152,w}, T. Wengler³⁰, S. Wenig³⁰, N. Vermes²¹, M. Werner⁴⁸, P. Werner³⁰, M. Werth¹⁶⁴, M. Wessels^{58a}, J. Wetter¹⁶², K. Whalen²⁹, A. White⁸, M.J. White⁸⁷, R. White^{32b}, S. White^{123a,123b}, D. Whiteson¹⁶⁴, D. Whittington⁶⁰, D. Wicke¹⁷⁶, F.J. Wickens¹³⁰, W. Wiedenmann¹⁷⁴, M. Wielers^{80,d}, P. Wienemann²¹, C. Wiglesworth³⁶, L.A.M. Wiik-Fuchs²¹, P.A. Wijeratne⁷⁷, A. Wildauer¹⁰⁰, M.A. Wildt^{42,t}, I. Wilhelm¹²⁸, H.G. Wilkens³⁰, J.Z. Will⁹⁹, E. Williams³⁵, H.H. Williams¹²¹, S. Williams²⁸, W. Willis^{35,*}, S. Willocq⁸⁵, J.A. Wilson¹⁸, A. Wilson⁸⁸, I. Wingerter-Seez⁵, S. Winkelmann⁴⁸, F. Winklmeier³⁰, M. Wittgen¹⁴⁴, T. Wittig⁴³, J. Wittkowski⁹⁹, S.J. Wollstadt⁸², M.W. Wolter³⁹, H. Wolters^{125a,h}, W.C. Wong⁴¹, G. Wooden⁸⁸, B.K. Wosiek³⁹, J. Wotschack³⁰, M.J. Woudstra⁸³, K.W. Wozniak³⁹, K. Wraight⁵³, M. Wright⁵³, B. Wrona⁷³, S.L. Wu¹⁷⁴, X. Wu⁴⁹, Y. Wu⁸⁸, E. Wulf³⁵, T.R. Wyatt⁸³, B.M. Wynne⁴⁶, S. Xella³⁶, M. Xiao¹³⁷, C. Xu^{33b,ab}, D. Xu^{33a}, L. Xu^{33b,ao}, B. Yabsley¹⁵¹, S. Yacoob^{146b,ap}, M. Yamada⁶⁵, H. Yamaguchi¹⁵⁶, Y. Yamaguchi¹⁵⁶, A. Yamamoto⁶⁵, K. Yamamoto⁶³, S. Yamamoto¹⁵⁶, T. Yamamura¹⁵⁶, T. Yamanaka¹⁵⁶, K. Yamauchi¹⁰², Y. Yamazaki⁶⁶, Z. Yan²², H. Yang^{33e}, H. Yang¹⁷⁴, U.K. Yang⁸³, Y. Yang¹¹⁰, Z. Yang^{147a,147b}, S. Yanush⁹², L. Yao^{33a}, Y. Yasu⁶⁵, E. Yatsenko⁴², K.H. Yau Wong²¹, J. Ye⁴⁰, S. Ye²⁵, A.L. Yen⁵⁷, E. Yildirim⁴², M. Yilmaz^{4b}, R. Yoosoofmiya¹²⁴, K. Yorita¹⁷², R. Yoshida⁶, K. Yoshihara¹⁵⁶, C. Young¹⁴⁴, C.J.S. Young¹¹⁹, S. Youssef²², D.R. Yu¹⁵, J. Yu⁸, J. Yu¹¹³, L. Yuan⁶⁶, A. Yurkewicz¹⁰⁷, B. Zabinski³⁹, R. Zaidan⁶², A.M. Zaitsev^{129,ac}, S. Zambito²³, L. Zanello^{133a,133b}, D. Zanzi¹⁰⁰, A. Zaytsev²⁵, C. Zeitnitz¹⁷⁶, M. Zeman¹²⁷, A. Zemla³⁹, O. Zenin¹²⁹, T. Ženiš^{145a}, D. Zerwas¹¹⁶, G. Zevi della Porta⁵⁷, D. Zhang⁸⁸, H. Zhang⁸⁹, J. Zhang⁶, L. Zhang¹⁵², X. Zhang^{33d}, Z. Zhang¹¹⁶, Z. Zhao^{33b}, A. Zhemchugov⁶⁴, J. Zhong¹¹⁹, B. Zhou⁸⁸, N. Zhou¹⁶⁴, C.G. Zhu^{33d}, H. Zhu⁴², J. Zhu⁸⁸, Y. Zhu^{33b},

X. Zhuang^{33a}, A. Zibell⁹⁹, D. Zieminska⁶⁰, N.I. Zimin⁶⁴, C. Zimmermann⁸²,
R. Zimmermann²¹, S. Zimmermann²¹, S. Zimmermann⁴⁸, Z. Zinonos^{123a,123b},
M. Ziolkowski¹⁴², R. Zitoun⁵, L. Živković³⁵, G. Zobernig¹⁷⁴, A. Zoccoli^{20a,20b},
M. zur Nedden¹⁶, G. Zurzolo^{103a,103b}, V. Zutshi¹⁰⁷, L. Zwalinski³⁰

- ¹ School of Chemistry and Physics, University of Adelaide, Adelaide, Australia
² Physics Department, SUNY Albany, Albany, NY, United States
³ Department of Physics, University of Alberta, Edmonton, AB, Canada
⁴ (a) Department of Physics, Ankara University, Ankara; (b) Department of Physics, Gazi University, Ankara; (c) Division of Physics, TOBB University of Economics and Technology, Ankara; (d) Turkish Atomic Energy Authority, Ankara, Turkey
⁵ LAPP, CNRS/IN2P3 and Université de Savoie, Annecy-le-Vieux, France
⁶ High Energy Physics Division, Argonne National Laboratory, Argonne, IL, United States
⁷ Department of Physics, University of Arizona, Tucson, AZ, United States
⁸ Department of Physics, The University of Texas at Arlington, Arlington, TX, United States
⁹ Physics Department, University of Athens, Athens, Greece
¹⁰ Physics Department, National Technical University of Athens, Zografou, Greece
¹¹ Institute of Physics, Azerbaijan Academy of Sciences, Baku, Azerbaijan
¹² Institut de Física d'Altes Energies and Departament de Física de la Universitat Autònoma de Barcelona, Barcelona, Spain
¹³ (a) Institute of Physics, University of Belgrade, Belgrade; (b) Vinca Institute of Nuclear Sciences, University of Belgrade, Belgrade, Serbia
¹⁴ Department for Physics and Technology, University of Bergen, Bergen, Norway
¹⁵ Physics Division, Lawrence Berkeley National Laboratory and University of California, Berkeley, CA, United States
¹⁶ Department of Physics, Humboldt University, Berlin, Germany
¹⁷ Albert Einstein Center for Fundamental Physics and Laboratory for High Energy Physics, University of Bern, Bern, Switzerland
¹⁸ School of Physics and Astronomy, University of Birmingham, Birmingham, United Kingdom
¹⁹ (a) Department of Physics, Bogazici University, Istanbul; (b) Department of Physics, Dogus University, Istanbul; (c) Department of Physics Engineering, Gaziantep University, Gaziantep, Turkey
²⁰ (a) INFN Sezione di Bologna; (b) Dipartimento di Fisica e Astronomia, Università di Bologna, Bologna, Italy
²¹ Physikalisches Institut, University of Bonn, Bonn, Germany
²² Department of Physics, Boston University, Boston, MA, United States
²³ Department of Physics, Brandeis University, Waltham, MA, United States
²⁴ (a) Universidade Federal do Rio De Janeiro COPPE/EE/IF, Rio de Janeiro; (b) Federal University of Juiz de Fora (UFJF), Juiz de Fora; (c) Federal University of Sao Joao del Rei (UFSJ), Sao Joao del Rei; (d) Instituto de Física, Universidade de Sao Paulo, Sao Paulo, Brazil
²⁵ Physics Department, Brookhaven National Laboratory, Upton, NY, United States
²⁶ (a) National Institute of Physics and Nuclear Engineering, Bucharest; (b) National Institute for Research and Development of Isotopic and Molecular Technologies, Physics Department, Cluj Napoca; (c) University Politehnica Bucharest, Bucharest; (d) West University in Timisoara, Timisoara, Romania
²⁷ Departamento de Física, Universidad de Buenos Aires, Buenos Aires, Argentina
²⁸ Cavendish Laboratory, University of Cambridge, Cambridge, United Kingdom
²⁹ Department of Physics, Carleton University, Ottawa, ON, Canada
³⁰ CERN, Geneva, Switzerland
³¹ Enrico Fermi Institute, University of Chicago, Chicago, IL, United States
³² (a) Departamento de Física, Pontificia Universidad Católica de Chile, Santiago; (b) Departamento de Física, Universidad Técnica Federico Santa María, Valparaíso, Chile
³³ (a) Institute of High Energy Physics, Chinese Academy of Sciences, Beijing; (b) Department of Modern Physics, University of Science and Technology of China, Anhui; (c) Department of Physics, Nanjing University, Jiangsu; (d) School of Physics, Shandong University, Shandong; (e) Physics Department, Shanghai Jiao Tong University, Shanghai, China
³⁴ Laboratoire de Physique Corpusculaire, Clermont Université and Université Blaise Pascal and CNRS/IN2P3, Clermont-Ferrand, France
³⁵ Nevis Laboratory, Columbia University, Irvington, NY, United States
³⁶ Niels Bohr Institute, University of Copenhagen, Copenhagen, Denmark
³⁷ (a) INFN Gruppo Collegato di Cosenza; (b) Dipartimento di Fisica, Università della Calabria, Rende, Italy
³⁸ (a) AGH University of Science and Technology, Faculty of Physics and Applied Computer Science, Krakow; (b) Marian Smoluchowski Institute of Physics, Jagiellonian University, Krakow, Poland
³⁹ The Henryk Niewodniczanski Institute of Nuclear Physics, Polish Academy of Sciences, Krakow, Poland
⁴⁰ Physics Department, Southern Methodist University, Dallas, TX, United States
⁴¹ Physics Department, University of Texas at Dallas, Richardson, TX, United States
⁴² DESY, Hamburg and Zeuthen, Germany
⁴³ Institut für Experimentelle Physik IV, Technische Universität Dortmund, Dortmund, Germany
⁴⁴ Institut für Kern- und Teilchenphysik, Technische Universität Dresden, Dresden, Germany
⁴⁵ Department of Physics, Duke University, Durham, NC, United States
⁴⁶ SUPA – School of Physics and Astronomy, University of Edinburgh, Edinburgh, United Kingdom
⁴⁷ INFN Laboratori Nazionali di Frascati, Frascati, Italy
⁴⁸ Fakultät für Mathematik und Physik, Albert-Ludwigs-Universität, Freiburg, Germany
⁴⁹ Section de Physique, Université de Genève, Geneva, Switzerland
⁵⁰ (a) INFN Sezione di Genova; (b) Dipartimento di Fisica, Università di Genova, Genova, Italy
⁵¹ (a) E. Andronikashvili Institute of Physics, Iv. Javakhishvili Tbilisi State University, Tbilisi; (b) High Energy Physics Institute, Tbilisi State University, Tbilisi, Georgia
⁵² Il Physikalisches Institut, Justus-Liebig-Universität Giessen, Giessen, Germany
⁵³ SUPA – School of Physics and Astronomy, University of Glasgow, Glasgow, United Kingdom
⁵⁴ Il Physikalisches Institut, Georg-August-Universität, Göttingen, Germany
⁵⁵ Laboratoire de Physique Subatomique et de Cosmologie, Université Joseph Fourier and CNRS/IN2P3 and Institut National Polytechnique de Grenoble, Grenoble, France
⁵⁶ Department of Physics, Hampton University, Hampton, VA, United States
⁵⁷ Laboratory for Particle Physics and Cosmology, Harvard University, Cambridge, MA, United States
⁵⁸ (a) Kirchhoff-Institut für Physik, Ruprecht-Karls-Universität Heidelberg, Heidelberg; (b) Physikalisches Institut, Ruprecht-Karls-Universität Heidelberg, Heidelberg; (c) ZITI Institut für technische Informatik, Ruprecht-Karls-Universität Heidelberg, Mannheim, Germany
⁵⁹ Faculty of Applied Information Science, Hiroshima Institute of Technology, Hiroshima, Japan
⁶⁰ Department of Physics, Indiana University, Bloomington, IN, United States

- ⁶¹ Institut für Astro- und Teilchenphysik, Leopold-Franzens-Universität, Innsbruck, Austria
- ⁶² University of Iowa, Iowa City, IA, United States
- ⁶³ Department of Physics and Astronomy, Iowa State University, Ames, IA, United States
- ⁶⁴ Joint Institute for Nuclear Research, JINR Dubna, Dubna, Russia
- ⁶⁵ KEK, High Energy Accelerator Research Organization, Tsukuba, Japan
- ⁶⁶ Graduate School of Science, Kobe University, Kobe, Japan
- ⁶⁷ Faculty of Science, Kyoto University, Kyoto, Japan
- ⁶⁸ Kyoto University of Education, Kyoto, Japan
- ⁶⁹ Department of Physics, Kyushu University, Fukuoka, Japan
- ⁷⁰ Instituto de Física La Plata, Universidad Nacional de La Plata and CONICET, La Plata, Argentina
- ⁷¹ Physics Department, Lancaster University, Lancaster, United Kingdom
- ⁷² ^(a) INFN Sezione di Lecce; ^(b) Dipartimento di Matematica e Fisica, Università del Salento, Lecce, Italy
- ⁷³ Oliver Lodge Laboratory, University of Liverpool, Liverpool, United Kingdom
- ⁷⁴ Department of Physics, Jožef Stefan Institute and University of Ljubljana, Ljubljana, Slovenia
- ⁷⁵ School of Physics and Astronomy, Queen Mary University of London, London, United Kingdom
- ⁷⁶ Department of Physics, Royal Holloway University of London, Surrey, United Kingdom
- ⁷⁷ Department of Physics and Astronomy, University College London, London, United Kingdom
- ⁷⁸ Louisiana Tech University, Ruston, LA, United States
- ⁷⁹ Laboratoire de Physique Nucléaire et de Hautes Energies, UPMC and Université Paris-Diderot and CNRS/IN2P3, Paris, France
- ⁸⁰ Fysiska institutionen, Lunds universitet, Lund, Sweden
- ⁸¹ Departamento de Física Teórica C-15, Universidad Autónoma de Madrid, Madrid, Spain
- ⁸² Institut für Physik, Universität Mainz, Mainz, Germany
- ⁸³ School of Physics and Astronomy, University of Manchester, Manchester, United Kingdom
- ⁸⁴ CPPM, Aix-Marseille Université and CNRS/IN2P3, Marseille, France
- ⁸⁵ Department of Physics, University of Massachusetts, Amherst, MA, United States
- ⁸⁶ Department of Physics, McGill University, Montreal, QC, Canada
- ⁸⁷ School of Physics, University of Melbourne, Victoria, Australia
- ⁸⁸ Department of Physics, The University of Michigan, Ann Arbor, MI, United States
- ⁸⁹ Department of Physics and Astronomy, Michigan State University, East Lansing, MI, United States
- ⁹⁰ ^(a) INFN Sezione di Milano; ^(b) Dipartimento di Fisica, Università di Milano, Milano, Italy
- ⁹¹ B.I. Stepanov Institute of Physics, National Academy of Sciences of Belarus, Minsk, Belarus
- ⁹² National Scientific and Educational Centre for Particle and High Energy Physics, Minsk, Belarus
- ⁹³ Department of Physics, Massachusetts Institute of Technology, Cambridge, MA, United States
- ⁹⁴ Group of Particle Physics, University of Montreal, Montreal, QC, Canada
- ⁹⁵ P.N. Lebedev Institute of Physics, Academy of Sciences, Moscow, Russia
- ⁹⁶ Institute for Theoretical and Experimental Physics (ITEP), Moscow, Russia
- ⁹⁷ Moscow Engineering and Physics Institute (MEPhI), Moscow, Russia
- ⁹⁸ D.V. Skobel'syn Institute of Nuclear Physics, M.V. Lomonosov Moscow State University, Moscow, Russia
- ⁹⁹ Fakultät für Physik, Ludwig-Maximilians-Universität München, München, Germany
- ¹⁰⁰ Max-Planck-Institut für Physik (Werner-Heisenberg-Institut), München, Germany
- ¹⁰¹ Nagasaki Institute of Applied Science, Nagasaki, Japan
- ¹⁰² Graduate School of Science and Kobayashi–Maskawa Institute, Nagoya University, Nagoya, Japan
- ¹⁰³ ^(a) INFN Sezione di Napoli; ^(b) Dipartimento di Scienze Fisiche, Università di Napoli, Napoli, Italy
- ¹⁰⁴ Department of Physics and Astronomy, University of New Mexico, Albuquerque, NM, United States
- ¹⁰⁵ Institute for Mathematics, Astrophysics and Particle Physics, Radboud University Nijmegen/Nikhef, Nijmegen, Netherlands
- ¹⁰⁶ Nikhef National Institute for Subatomic Physics and University of Amsterdam, Amsterdam, Netherlands
- ¹⁰⁷ Department of Physics, Northern Illinois University, DeKalb, IL, United States
- ¹⁰⁸ Budker Institute of Nuclear Physics, SB RAS, Novosibirsk, Russia
- ¹⁰⁹ Department of Physics, New York University, New York, NY, United States
- ¹¹⁰ Ohio State University, Columbus, OH, United States
- ¹¹¹ Faculty of Science, Okayama University, Okayama, Japan
- ¹¹² Homer L. Dodge Department of Physics and Astronomy, University of Oklahoma, Norman, OK, United States
- ¹¹³ Department of Physics, Oklahoma State University, Stillwater, OK, United States
- ¹¹⁴ Palacký University, RCPTM, Olomouc, Czech Republic
- ¹¹⁵ Center for High Energy Physics, University of Oregon, Eugene, OR, United States
- ¹¹⁶ LAL, Université Paris-Sud and CNRS/IN2P3, Orsay, France
- ¹¹⁷ Graduate School of Science, Osaka University, Osaka, Japan
- ¹¹⁸ Department of Physics, University of Oslo, Oslo, Norway
- ¹¹⁹ Department of Physics, Oxford University, Oxford, United Kingdom
- ¹²⁰ ^(a) INFN Sezione di Pavia; ^(b) Dipartimento di Fisica, Università di Pavia, Pavia, Italy
- ¹²¹ Department of Physics, University of Pennsylvania, Philadelphia, PA, United States
- ¹²² Petersburg Nuclear Physics Institute, Gatchina, Russia
- ¹²³ ^(a) INFN Sezione di Pisa; ^(b) Dipartimento di Fisica E. Fermi, Università di Pisa, Pisa, Italy
- ¹²⁴ Department of Physics and Astronomy, University of Pittsburgh, Pittsburgh, PA, United States
- ¹²⁵ ^(a) Laboratório de Instrumentação e Física Experimental de Partículas – LIP, Lisboa, Portugal; ^(b) Departamento de Física Teórica y del Cosmos and CAFPE, Universidad de Granada, Granada, Spain
- ¹²⁶ Institute of Physics, Academy of Sciences of the Czech Republic, Praha, Czech Republic
- ¹²⁷ Czech Technical University in Prague, Praha, Czech Republic
- ¹²⁸ Faculty of Mathematics and Physics, Charles University in Prague, Praha, Czech Republic
- ¹²⁹ State Research Center Institute for High Energy Physics, Protvino, Russia
- ¹³⁰ Particle Physics Department, Rutherford Appleton Laboratory, Didcot, United Kingdom
- ¹³¹ Physics Department, University of Regina, Regina, SK, Canada
- ¹³² Ritsumeikan University, Kusatsu, Shiga, Japan
- ¹³³ ^(a) INFN Sezione di Roma I; ^(b) Dipartimento di Fisica, Università La Sapienza, Roma, Italy
- ¹³⁴ ^(a) INFN Sezione di Roma Tor Vergata; ^(b) Dipartimento di Fisica, Università di Roma Tor Vergata, Roma, Italy
- ¹³⁵ ^(a) INFN Sezione di Roma Tre; ^(b) Dipartimento di Matematica e Fisica, Università Roma Tre, Roma, Italy
- ¹³⁶ ^(a) Faculté des Sciences Ain Chock, Réseau Universitaire de Physique des Hautes Energies – Université Hassan II, Casablanca; ^(b) Centre National de l'Energie des Sciences Techniques Nucleaires, Rabat; ^(c) Faculté des Sciences Semlalia, Université Cadi Ayyad, LPHEA, Marrakech; ^(d) Faculté des Sciences, Université Mohamed Premier and LPTPM, Oujda; ^(e) Faculté des sciences, Université Mohammed V-Agdal, Rabat, Morocco

- ¹³⁷ DSM/IRFU (Institut de Recherches sur les Lois Fondamentales de l'Univers), CEA Saclay (Commissariat à l'Energie Atomique et aux Energies Alternatives), Gif-sur-Yvette, France
- ¹³⁸ Santa Cruz Institute for Particle Physics, University of California Santa Cruz, Santa Cruz, CA, United States
- ¹³⁹ Department of Physics, University of Washington, Seattle, WA, United States
- ¹⁴⁰ Department of Physics and Astronomy, University of Sheffield, Sheffield, United Kingdom
- ¹⁴¹ Department of Physics, Shinshu University, Nagano, Japan
- ¹⁴² Fachbereich Physik, Universität Siegen, Siegen, Germany
- ¹⁴³ Department of Physics, Simon Fraser University, Burnaby, BC, Canada
- ¹⁴⁴ SLAC National Accelerator Laboratory, Stanford, CA, United States
- ¹⁴⁵ ^(a) Faculty of Mathematics, Physics & Informatics, Comenius University, Bratislava; ^(b) Department of Subnuclear Physics, Institute of Experimental Physics of the Slovak Academy of Sciences, Kosice, Slovak Republic
- ¹⁴⁶ ^(a) Department of Physics, University of Cape Town, Cape Town; ^(b) Department of Physics, University of Johannesburg, Johannesburg; ^(c) School of Physics, University of the Witwatersrand, Johannesburg, South Africa
- ¹⁴⁷ ^(a) Department of Physics, Stockholm University; ^(b) The Oskar Klein Centre, Stockholm, Sweden
- ¹⁴⁸ Physics Department, Royal Institute of Technology, Stockholm, Sweden
- ¹⁴⁹ Departments of Physics & Astronomy and Chemistry, Stony Brook University, Stony Brook, NY, United States
- ¹⁵⁰ Department of Physics and Astronomy, University of Sussex, Brighton, United Kingdom
- ¹⁵¹ School of Physics, University of Sydney, Sydney, Australia
- ¹⁵² Institute of Physics, Academia Sinica, Taipei, Taiwan
- ¹⁵³ Department of Physics, Technion: Israel Institute of Technology, Haifa, Israel
- ¹⁵⁴ Raymond and Beverly Sackler School of Physics and Astronomy, Tel Aviv University, Tel Aviv, Israel
- ¹⁵⁵ Department of Physics, Aristotle University of Thessaloniki, Thessaloniki, Greece
- ¹⁵⁶ International Center for Elementary Particle Physics and Department of Physics, The University of Tokyo, Tokyo, Japan
- ¹⁵⁷ Graduate School of Science and Technology, Tokyo Metropolitan University, Tokyo, Japan
- ¹⁵⁸ Department of Physics, Tokyo Institute of Technology, Tokyo, Japan
- ¹⁵⁹ Department of Physics, University of Toronto, Toronto, ON, Canada
- ¹⁶⁰ ^(a) TRIUMF, Vancouver, BC; ^(b) Department of Physics and Astronomy, York University, Toronto, ON, Canada
- ¹⁶¹ Faculty of Pure and Applied Sciences, University of Tsukuba, Tsukuba, Japan
- ¹⁶² Department of Physics and Astronomy, Tufts University, Medford, MA, United States
- ¹⁶³ Centro de Investigaciones, Universidad Antonio Narino, Bogota, Colombia
- ¹⁶⁴ Department of Physics and Astronomy, University of California Irvine, Irvine, CA, United States
- ¹⁶⁵ ^(a) INFN Gruppo Collegato di Udine; ^(b) ICTP, Trieste; ^(c) Dipartimento di Chimica, Fisica e Ambiente, Università di Udine, Udine, Italy
- ¹⁶⁶ Department of Physics, University of Illinois, Urbana, IL, United States
- ¹⁶⁷ Department of Physics and Astronomy, University of Uppsala, Uppsala, Sweden
- ¹⁶⁸ Instituto de Física Corpuscular (IFIC) and Departamento de Física Atómica, Molecular y Nuclear and Departamento de Ingeniería Electrónica and Instituto de Microelectrónica de Barcelona (IMB-CNM), University of Valencia and CSIC, Valencia, Spain
- ¹⁶⁹ Department of Physics, University of British Columbia, Vancouver, BC, Canada
- ¹⁷⁰ Department of Physics and Astronomy, University of Victoria, Victoria, BC, Canada
- ¹⁷¹ Department of Physics, University of Warwick, Coventry, United Kingdom
- ¹⁷² Waseda University, Tokyo, Japan
- ¹⁷³ Department of Particle Physics, The Weizmann Institute of Science, Rehovot, Israel
- ¹⁷⁴ Department of Physics, University of Wisconsin, Madison, WI, United States
- ¹⁷⁵ Fakultät für Physik und Astronomie, Julius-Maximilians-Universität, Würzburg, Germany
- ¹⁷⁶ Fachbereich C Physik, Bergische Universität Wuppertal, Wuppertal, Germany
- ¹⁷⁷ Department of Physics, Yale University, New Haven, CT, United States
- ¹⁷⁸ Yerevan Physics Institute, Yerevan, Armenia
- ¹⁷⁹ Centre de Calcul de l'Institut National de Physique Nucléaire et de Physique des Particules (IN2P3), Villeurbanne, France

^a Also at Department of Physics, King's College London, London, United Kingdom.

^b Also at Laboratório de Instrumentação e Física Experimental de Partículas – LIP, Lisboa, Portugal.

^c Also at Faculdade de Ciências and CFNUL, Universidade de Lisboa, Lisboa, Portugal.

^d Also at Particle Physics Department, Rutherford Appleton Laboratory, Didcot, United Kingdom.

^e Also at TRIUMF, Vancouver, BC, Canada.

^f Also at Department of Physics, California State University, Fresno, CA, United States.

^g Also at Novosibirsk State University, Novosibirsk, Russia.

^h Also at Department of Physics, University of Coimbra, Coimbra, Portugal.

ⁱ Also at Università di Napoli Parthenope, Napoli, Italy.

^j Also at Institute of Particle Physics (IPP), Canada.

^k Also at Department of Physics, Middle East Technical University, Ankara, Turkey.

^l Also at Louisiana Tech University, Ruston, LA, United States.

^m Also at Departamento de Física and CEFITEC of Faculdade de Ciências e Tecnologia, Universidade Nova de Lisboa, Caparica, Portugal.

ⁿ Also at Department of Physics and Astronomy, Michigan State University, East Lansing, MI, United States.

^o Also at Department of Financial and Management Engineering, University of the Aegean, Chios, Greece.

^p Also at Institutio Catalana de Recerca i Estudis Avancats, ICREA, Barcelona, Spain.

^q Also at Department of Physics, University of Cape Town, Cape Town, South Africa.

^r Also at Institute of Physics, Azerbaijan Academy of Sciences, Baku, Azerbaijan.

^s Also at CERN, Geneva, Switzerland.

^t Also at Institut für Experimentalphysik, Universität Hamburg, Hamburg, Germany.

^u Also at Manhattan College, New York, NY, United States.

^v Also at Institute of Physics, Academia Sinica, Taipei, Taiwan.

^w Also at School of Physics and Engineering, Sun Yat-sen University, Guanzhou, China.

^x Also at Academia Sinica Grid Computing, Institute of Physics, Academia Sinica, Taipei, Taiwan.

^y Also at Laboratoire de Physique Nucléaire et de Hautes Energies, UPMC and Université Paris-Diderot and CNRS/IN2P3, Paris, France.

^z Also at School of Physical Sciences, National Institute of Science Education and Research, Bhubaneswar, India.

^{aa} Also at Dipartimento di Fisica, Università La Sapienza, Roma, Italy.

^{ab} Also at DSM/IRFU (Institut de Recherches sur les Lois Fondamentales de l'Univers), CEA Saclay (Commissariat à l'Energie Atomique et aux Energies Alternatives), Gif-sur-Yvette, France.

- ^{ac} Also at Moscow Institute of Physics and Technology State University, Dolgoprudny, Russia.
- ^{ad} Also at Section de Physique, Université de Genève, Geneva, Switzerland.
- ^{ae} Also at Departamento de Física, Universidade de Minho, Braga, Portugal.
- ^{af} Also at Department of Physics, The University of Texas at Austin, Austin, TX, United States.
- ^{ag} Also at Institute for Particle and Nuclear Physics, Wigner Research Centre for Physics, Budapest, Hungary.
- ^{ah} Also at DESY, Hamburg and Zeuthen, Germany.
- ^{ai} Also at International School for Advanced Studies (SISSA), Trieste, Italy.
- ^{aj} Also at Department of Physics and Astronomy, University of South Carolina, Columbia, SC, United States.
- ^{ak} Also at Faculty of Physics, M.V. Lomonosov Moscow State University, Moscow, Russia.
- ^{al} Also at Nevis Laboratory, Columbia University, Irvington, NY, United States.
- ^{am} Also at Physics Department, Brookhaven National Laboratory, Upton, NY, United States.
- ^{an} Also at Department of Physics, Oxford University, Oxford, United Kingdom.
- ^{ao} Also at Department of Physics, The University of Michigan, Ann Arbor, MI, United States.
- ^{ap} Also at Discipline of Physics, University of KwaZulu-Natal, Durban, South Africa.
- * Deceased.